NOVEL PHASE NOISE COMPENSATION SCHEMES

FOR COMMUNICATION TRANSCEIVERS

by

Liang Zhao

A Dissertation Presented to the
FACULTY OF THE GRADUATE SCHOOL
UNIVERSITY OF SOUTHERN CALIFORNIA
In Partial Fulfillment of the
Requirements for the Degree
DOCTOR OF PHIILOSOPHY
(ELECTRICAL ENGINEERING)

December 2006

Acknowledgements

First of all, I am grateful to my academic advisor Dr. Won Namgoong for his constant encouragement, support and guidance during the past five years. The work presented here could not have been accomplished without the inspiring discussions with him in each stage of the research, from the brainstorming of the ideas, to the formation of the theoretical framework, up to the final validation of the theory on a real oscillator. I also want to acknowledge the financial support from the Semiconductor Research Corporation (SRC) and the National Science Foundation (NSF).

I would like to thank Dr. Robert A. Scholtz for providing a wonderful environment and state-of-the-art laboratory facilities at the Ultra Lab. I would also like to thank my academic advisory committee members: Dr. William C. Lindsey, Dr. Antonio Ortega, and Dr. Robert A. Scholtz from the Dept. of Electrical Engineering (EE), and Dr. Dr. Kenneth Alexander from the Dept. of Mathematics, for their valuable advice and opinions. I also had the great pleasures to work with Mr. Gandhi Puvvada, Dr. Ubashi Mitra, Dr. Krishna Nayak, and Dr. Todd Brun as a TA or grader.

Special thanks will go to my former advisor Dr. Moeness Amin from the Dept. of Electrical and Computer Engineering at Villanova University, for guiding me into the research area of signal processing and communications. My understanding of communication systems also benefits a lot from the excellent course and projects taught by Dr. Kevin Buckley at Villanova University.

I am greatly indebted to the members of the research group: Shaomin Hsu, Kyongsu Lee, Lei Feng, Sotirios Zogopoulos, Ali Medi, and Jongrit Lerdworatawee, for their helpful discussions and close collaboration. Thanks Sotirios for providing the oscillator. Thanks Shaomin, Ali, and Kyongsu for introducing the RF laboratory to me. Thanks Lei, Shaomin, Kyongsu, and Jongrit for the fun discussions and various timely help. The same gratitude also goes to former laboratory members at Villanova: Dr. Yimin Zhang, Weifeng Mu, Lin He, Ce Zhang, and Huangfeng Zhang.

The USC EE department not only provides excellent faculty and staff, but also excellent graduate students. I am fortunate to know so many talented friends and classmates from EE: Dr. Lei Zhuge, Dr. Mingrui Zhu, Dr. Jun Yang, Dr. Yuankai Wang, Dr. Zhourong Miao, Dr. Shan Liu, Dr. Fang Liu, Dr. Jifeng Geng, Dr. Quangzheng Li, Dr. Yan Wang, Zheng Li, Xiaofeng Wang, Jiansong Chen, Ding Tian, Leanne Chan, Dr. Yang Yu, Dr. Bo Hong, Ran Cao, Dr. Hua Yang, Bo Zhang, Li Zhang, Xijin (Eric) Yan, Dr. Hesu Huang, Yining Liu, Ide Huang, Feilong Liu and Jordan Melzer. USC has a lively and balanced campus and my horizon was broadened from knowing many non-EE friends: Xiaofei Wang, Sarah Sang, Gang Xiong, Lijuan Mo, Shan Gao, Zhigang Deng, Xinmin He, Amy Gussin, Xin Gao, Tracy Ou, Xi Xu, Yuan Wang, Weihong Xu, Ming Li, Hui Zhou, Jie Situ, Manlin Wang, Hui Zhang, Jing Chen, Yu Yang, Xiaobo Liu, Haoyuan Liu, Ting Wang, Will (Wei) Lu, Harrison (Hai) Wu. I owe a huge gratitude to my friends for making my graduate student life at USC less miserable and more enjoyable.

During the summer of 2005, I spent a rewarding summer as an intern at the Bosch Research Center at Palo Alto, CA. I owe my sincere gratefulness to Mr. Jingao Wang and Dr. Lucas Marti for help me understand better the GPS systems and the Kalman filter. The friendly colleagues and staff at Bosch also impressed me and made my stay there pleasant.

The last and the deepest, I want to thank my family members. Wendy has been a constant source of love, encouragement, and support during my entire Ph.D. student life. I can also always felt the love and support from my parents and my sister Hua, even though they have been thousands of miles away in China. I also want to thank my other family members for their supports during all the years.

Table of Contents

List of Figures

Abstract

Local oscillators are prevalent in most communication systems. They upconvert the baseband signals to the radio frequency (RF) at the transmitter, or downconvert the RF signals to intermediate frequency or baseband. Local oscillators suffer from a type of noises know as the phase noises (PHN). Since the performance of the local oscillators is crucial to the performance of the whole communication system, it is important to compensate the effects of the phase noise originated from the local oscillators. In this research, novel PHN compensation methods are proposed for both communication receivers and transmitters. The proposed approach uses the information provided by an additional signal path that is added with modest hardware overhead to better estimate the PHN.

For receivers, the oscillator output in this additional signal path is self-downconverted to the baseband by mixing itself with a delayed and conjugated replica so as to provide PHN information that is free from data-modulation. A joint prediction and smoothing Wiener filter can then be employed to obtain the minimum mean-squared error (MMSE) estimate of the PHN. Adaptive schemes are also presented using the least-mean-square (LMS) algorithm and recursive-least-square (RLS) algorithm. Simulations of a 64-QAM receiver confirm the analysis results of the PHN estimation performance, and show that the proposed method can improve the receiver performance significantly over the conventional schemes. Lab testing

results for a BPSK receiver is also provided which suggests that the proposed scheme outperforms the conventional schemes.

The concept of self-downconversion is applied to the transmitter PHN compensation as well. It differs from the receiver PHN compensation in that two self-downconversion blocks are employed for transmitters, one to obtain a baseband PHN signal and one to obtain an estimation error signal. The adaptive transmitter PHN estimation algorithm is devised and simulated. The improvement in PHN spectrum can be as high as 10 dB.

There are generally two types of PHN models commonly used in the literature: the stationary PHN and the Wiener PHN. Both types of PHN can be compensated effectively by the proposed approaches.

Chapter 1

Introduction

In communication systems, oscillators are used extensively at both the transmitters and the receivers [37]. Ideally, an oscillator generates a sinusoidal signal at its output. At the transmitters, communication signals at the baseband are upconverted to the radio frequency (RF) by mixing itself with the local oscillator output. Similarly, the RF signal received by the receiver is down-converted to baseband or intermediate frequency (IF) by a mixer with the local oscillator as the other input.

A problem of crucial importance to communication systems is the stability of oscillators. The oscillator instability due to noise, which manifests itself as phase noise (PHN), is one of the primary factors that limit the achievable performance in many communication systems [1][9][14][22][25][33][39][44][45]. This is especially true when integrated oscillators are employed [23][39]. Although many high quality off-chip oscillators are available, it is often preferable from both a cost and power perspective to employ noisier on-chip oscillators. Consequently, considerable effort has been expended in minimizing the performance degradation caused by PHN.

The existing work in this area has taken two distinct approaches. In the first approach, the PHN of the local oscillator itself was minimized by making appropriate circuit level design choices. To understand the mechanism of the PHN generated in oscillator circuits, it is important to recognize how the various sources of noise in

the oscillator circuits are transformed into PHN [17][19][24][27][38][39]. Factors including the carrier frequency, the power dissipation, resonator Q (quality factor) and ambient noise are identified to be key parameters and efforts have been expended to improve these parameters.

The other approach to combat PHN, carried out on a system level, mainly resorts to signal processing techniques to compensate for the effects of the PHN of a given oscillator. Traditional approaches to combat PHN are based on conventional feedback tracking schemes and per-survivor processing techniques [43]. Adaptive PHN estimation methods were first proposed in [16] and [10], where the PHN is corrected by an adaptive prediction filter. Adaptive PHN estimation with the aid of pilot symbols (or pilot subcarrier in OFDM) was suggested in [43] and [32]. Maximum-likelihood (ML) non-pilot-based PHN compensation schemes were suggested for OFDM in [30].

In this work, a novel approach is proposed to compensate the PHN [49][50][51][52]. In contrast to many of the existing approaches for combating phase noise, we propose to use signal processing techniques together with circuit techniques to overcome the phase noise problems. The basic concept for the receiver PHN compensation, similar to the transmitter counterpart, is to modify the receiver analog front-end by adding an additional signal path directly from the oscillator, so as to provide a non-data modulated observation of the PHN. This enables the PHN to be estimated by a smoothing filter (a filter that employs both past and future information), instead of a conventional prediction filter (a filter that only uses past

information). The hardware overhead of introducing this additional path in the analog front-end is modest, especially in an integrated circuit.

At the receiver, the information provided by the additional signal path allows a joint prediction and smoothing Wiener filter that optimally estimates the PHN in the minimum mean-squared error (MMSE) sense. The PHN is generally modeled as a wide sense stationary Gaussian process or a Wiener process [33][27][13]. Performance of the proposed scheme, in terms of the PHN estimation error variance and the signal-to-noise ratio (SNR) after PHN compensation, is analyzed for both types of PHN. Significant improvement in performance over conventional approaches is observed. Since the spectrum of the oscillator PHN is generally unknown at design time and varies with the operating environment, adaptive estimation filters based on decision-directed least-mean-square (LMS) and recursive least-square (RLS) filters are developed. Simulation results for a 64-QAM receiver employing the proposed scheme are presented, demonstrating that the proposed scheme can combat both types of PHN very effectively. Lab testing results for a BPSK receiver employing a noisy ring oscillator are also shown, validating the effectiveness of the proposed approach on the practical PHN.

The self-downconversion idea for receivers can be modified to compensate oscillator PHN in transmitters as well. A self-downconversion transmitter scheme is proposed that can reduce transmitter PHN effectively. Although the motivation for a second path directly from the oscillator is the same as that for receivers, the transmitter PHN compensation differ itself from the receiver case in several aspects. Firstly,

with only an additional path from oscillator, it is difficult to obtain an effective PHN error to drive an adaptive PHN estimation filter. Another self-downconversion block is therefore added to the transmitted signal that enables to form the PHN error. Secondly, the goal for transmitter PHN compensation allows a constant difference between the actual PHN and the PHN estimate used in compensation. Thirdly, there is no channel noise present in the transmitter, therefore, channel noise effects can be ignored and the only noise source is from the quantization.

Although some overhead is introduced, the proposed approach can relax the design requirement of the oscillator in the analogue domain and allow the usage of a noisier oscillator, enabling overall simplification in the analogue domain. Thanks to the powerful VLSI technology, powerful signal processing techniques can be applied to estimate and compensate for the PHN in the digital domain, which is much easier to implement than designing and fine tuning a high quality oscillator. The motivation is to shift the task of analogue design to digital signal processing. This follows the observation that the digital VLSI technology has advanced tremendously while good analogue designs still rely on the “art” or “craftsmanship” of the experienced analogue designers.

This dissertation is organized as follows. Background on oscillator PHN and mathematical models are introduced in Chapter 2. Chapter 3 introduces the architecture of PHN compensation receiver, in which both conventional and proposed schemes are included. The optimum PHN estimation methods are discussed in Chapter 4 for both the stationary PHN and the Wiener PHN. In the analysis devel-

oped in Chapter 4, the knowledge of some statistical properties of PHN is assumed. This prior knowledge is removed in Chapter 6, where adaptive schemes are introduced, and some lab testing results for receiver PHN compensation are presented. The PHN estimation method and the performance for transmitters are provided in Chapter 7 and Chapter 8, respectively. Conclusions are drawn in Chapter 10.

Chapter 2

Background on Phase Noise

2.1 Phase Noise Concepts

In communication receivers, the sinusoidal signals generated by the LO are used to downconvert the passband signal to an intermediate frequency or to the baseband. The output of a practical LO, however, is not a perfect sinusoid. Instead of being an ideal impulse at the carrier frequency, the spectrum of a real LO output is spread and has a skirt shape, as shown in Figure 1

Although circuit and device noises in an oscillator can perturb both the amplitude and the phase of the oscillator output, the deviation in the amplitude is mostly negligible because the amplitude is often limited by automatic level control (ALC) in the oscillator [18][39]. The problem of major concern remains in the phase of the oscillator output. As such, the practical oscillator output can be written as $\cos(\omega_o t + \theta(t))$, instead of an ideal sinusoidal output $\cos(\omega_o t)$, where ω_o is the oscillation frequency and $\theta(t)$ is the phase noise. The time varying phase noise $\theta(t)$ is often treated as a random process representing variations in the sinusoidal period. The detailed models of $\theta(t)$ will be introduced later in this chapter.

One consequence of the variation in the oscillator period variation is the small random deviation of the zero-crossing points in time domain. The term jitter is often

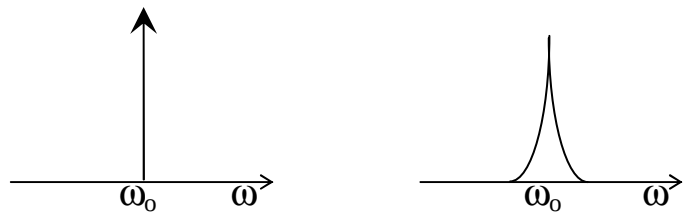

Figure 1. Spectrum of ideal and actual oscillator outputs

used to quantify this deviation. Although phase and jitter are often used interchangeably in literature, phase noise emphasize the spectral properties of an oscillator from a frequency domain view, while jitter is treated more in time domain as a measure of the timing accuracy. Both phase noise and jitter characterize the noisy properties of the oscillator and sometimes it is important to convert one to the other. Poore provided a good review of the relationship between phase noise and jitter [35] and more related work can be found in [11][15][31][42]. It is beneficial to realize the close link between phase noise and jitter to obtain a complete understanding of the problem.

2.2 The Effects of Phase Noise

To understand the importance of phase noise in RF communication receives, consider a generic receiver as shown in Figure 2, where a local oscillator is mixed with the received signal. The mixing operation is equivalent to convolving the incoming signal spectrum with the oscillator spectrum in the frequency domain. When an ideal mixer is employed, the received signal spectrum is simply shifted by

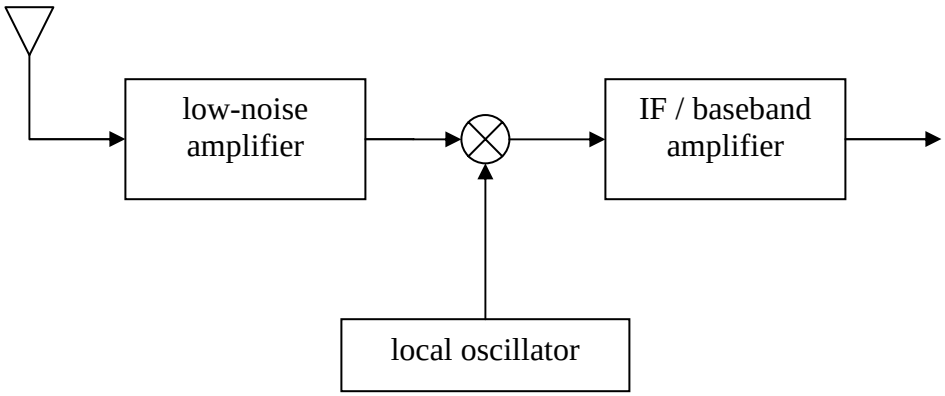

Figure 2. A block diagram of a generic receiver

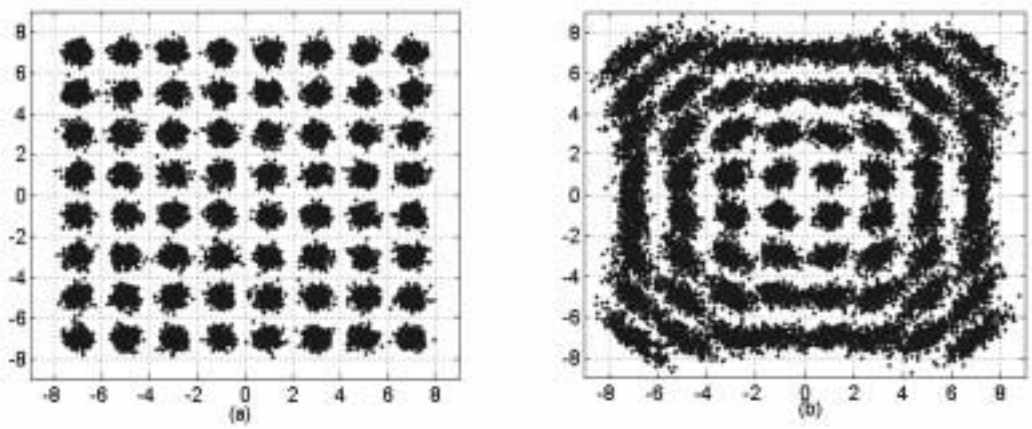

Figure 3. Constellation of 64 QAM. (a) without PHN. (b) with PHN.

the frequency of the local oscillator. In an actual oscillator with phase noise present, however, the frequency translation also corrupts the information carried in the phase of the signal carrier. This is especially problematic in communication systems operating with large signal constellations. For example. the downconversion of a 64-QAM waveform by a mixer that is driven by a

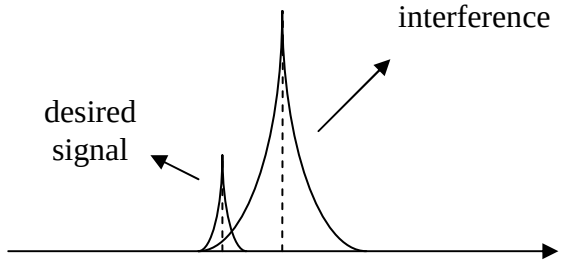

Figure 4. Effect of reciprocal mixing.

noiseless and noisy local oscillator results in the constellations as show in Figure 3(a) and Figure 3(b), respectively. As evident from these plots, the bit error rate of the receiver with noisy local oscillator increases significantly.

Even in communication systems with small signal constellations (e.g. QPSK), the phase noise can result in significant performance degradation if the desired received signal is accompanied by a large interferer in an adjacent channel. The convolution of the adjacent interferer with the noisy local oscillator in the frequency domain causes the downconverted band to consist of two overlapping spectra with the desired signal suffering from significant noise due to the tail of the interferer. This effect, which is referred to “reciprocal mixing” [39], is illustrated in Figure 4.

Recently, the multicarrier transmission technique know as orthogonal frequency division multiplexing (OFDM) has drawn considerable attention in broadband wireless and broadcasting applications [5][6][8][47]. Powered with the techniques known as circular prefix [5][26], OFDM can ease the computationally expensive task of equalization in broadband wireless communication channels by single tap equalizers. This is achieved by dividing the wide bandwidth of the chan-

nel into subchannels and sending data at a lower rate parallelly in the narrowband subchannels. One of the drawbacks of the OFDM system is that it is highly sensitive to synchronization errors and phase noise [3][5][33][34][46]. This can be understood intuitively: when the number of subchannels becomes large, the bandwidth of each subchannel becomes so narrow that the phase noise of the oscillator can no longer be considered as an ideal impulse in frequency domain.

2.3 Phase Noise Mechanism

The frequency of the local oscillator is usually adjustable in a RF receiver in well defined steps over a frequency band of interest. This function is typically achieved using a phase-locked loop (PLL), which includes as one of its main building blocks a voltage controlled oscillator (VCO). The VCO, which is an oscillator whose frequency is set by its input voltage signal, is often the main factor limiting the sensitivity of many integrated receivers. From the cost and size perspective, it is highly desirable to integrate the VCO with the rest of the receiver on a single chip as it removes off-chip resonator and discrete inductors.

One of the drawbacks of a fully integrated VCO is the low quality factors of the resonators compared to discrete devices, resulting in comparatively large phase noise levels. Consequently, the availability of high quality on-chip inductors and varactors, both of which are commonly used in realizing the VCO, is crucial to the design of high performance oscillators. Significant research has been expended on improving the quality factor of the on-chip inductors [4][48]. The quality factor Q of

on-chip inductors, however, still remain relatively low with typical values of around 10, which is significantly lower than their discrete counterparts with a Q value of 50 or above. The main challenge in the design of varactors has been in maintaining their tuning range despite the reduction in supply voltage caused by continued scaling of process technology [2][7]

In addition to improving the components of the oscillator, and active research area has been on understanding the fundamental mechanisms governing the process by which the various noise sources turn into phase noise. Better understanding of phase noise mechanism has led to designs with improved phase noise performance. In circuit society, the PHN has been investigated for over three decades and a large amount of literature is available. To name a few, [13][17][24][27][38][39][41] provide important understandings of phase noise mechanism. The accumulated research results can be roughly categorized into three classes.

In the first and classical class of work, linear time-invariant (LTI) analysis are applied to oscillators [24][38][39]. Based on the observations of phase noise spectrum, Leeson heuristically derived the famous Leeson's phase noise model without rigid proof [24]. Leeson's model states that the phase noise spectrum is composed of three regions: $1/f^3$ region at small frequency offsets, $1/f^2$ region up to half bandwidth of the feedback loop, and above that point a flat spectrum floor. Using the feedback approach, Razavi derived Leeson's equation (the middle region) by approximate the transfer function of the loop in the vicinity of the oscillation frequency using Taylor expansion [38][39]. The circuit and device noises in the oscillator are shaped by the

transfer function and thus spectrally resemble the transfer function. These results provide insights into the mechanism of phase noise, and reveal the dependence of the phase noise upon the quality factor Q of the LC tank, the oscillation frequency, and the offset frequency. Designers can improve their oscillator design by taking these factors into consideration.

The second class of phase noise models is based on linear time-varying analysis. Although LTI approach and Leeson's model are simple and thus attractive, it includes some parameters that must be determined from measurements, diminishing the predictive power. Upon examining the assumptions, Hajimiri and Lee asserted that the time-invariance property does not hold for oscillators and proposed a LTV approach [17][18][19][23]. They defined a time-varying impulse sensitivity function (ISF, mostly measured from simulation), which has a similar role to the transfer function in LTI approach. The ISF is periodic and suggests that there are sensitive and insensitive moments in an oscillation cycle. The noises in circuits are then convolved with the ISF to obtain the output spectrum. This LTV approach can calculate some phase noise spectral parameters that can not be predicted by Leeson's model.

The LTV approach was again challenged by Demir, Mehrotra, and Roychowdhury [12][13][27]. They argue that the linear approach is not valid, and use the state equation formulation to describe the dynamics of the oscillator, and derived the phase noise spectral properties using stochastic differential equations. The derivation is mathematically intensive in this approach and does not provide as much

insights as the LTI and LTV approach. However, the key result is important: the oscillator output has a Lorentzian spectrum, i.e., the shape of the magnitude of a one-pole lowpass filter transfer function. The Lorentzian spectrum result has a finite power at the oscillation frequency and thus avoids the singularity in other PHN models.

2.4 Mathematical Models for Phase Noise

Although PHN specification of an oscillator is often provided in frequency domain, it is helpful for system level analysis to have a time domain model of PHN. As stated earlier, there are two commonly used mathematical models of PHN: stationary PHN and Wiener PHN [13][33][40]. Communication signals and systems are often analyzed in the form of baseband representation for simplicity [36]. The LO output in baseband complex form can be expressed as $e^{j\theta(t)}$, where $\theta(t)$ is the time-varying phase. Without loss of generality, the initial phase of the carrier can be assumed to be zero herein for simplicity. Accordingly, $\theta(t)$, which represents the difference between the carrier phase and the phase of the LO output, should be correctly estimated and compensated.

When the LO output is phase-locked, $\theta(t)$ can be modeled as a stationary PHN:

$$\theta(t) = \theta_o + \phi(t), \tag{1}$$

where θ_o is a constant phase difference, and $\phi(t)$ is a zero-mean, wide sense stationary (WSS), colored Gaussian process. Since $\phi(t)$ is the jitter in a phase-locked

oscillator, $\phi(t)$ remains small and $\phi(t) << 1$. Therefore, LO output $e^{j\theta(t)}$ approximates to

$$e^{j\theta(t)} \approx e^{j\theta_o}(1 + j\phi(t)), \tag{2}$$

With (2), the power spectrum density (PSD) of the LO output $S(f)$ can be approximated as $S(f) \approx \delta(f) + S_\phi(f)$, which states that $S(f)$ is identical to $S_\phi(f)$ except for the Dirac pulse [33][43][40]. For the Lorentzian PHN model, the autocorrelation of PHN $\phi(t)$ is

$$R_\phi(\tau) = \sigma_\phi^2 e^{-\alpha|\tau|}, \tag{3}$$

where σ_ϕ^2 is the variance of PHN and α determines the 3 dB bandwidth of the PHN PSD. The corresponding PSD in frequency f (Hz) is

$$S_\phi(f) = \left(\frac{\sigma_\phi^2}{\pi B_\phi}\right) \Bigg/ \left(1 + \left(\frac{f}{B_\phi}\right)^2\right), \tag{4}$$

where $B_\phi = \alpha/2\pi$. It is clear from the above that the parameters describing the stationary PHN are σ_ϕ^2 and α (or B_ϕ). This model ignores the noise floor in the PHN PSD, which can be easily included by adding a delta function in (3) or a constant in (4).

When the LO is only frequency-locked (e.g., a free-running oscillator), the time-varying phase $\theta(t)$ is modeled as a Wiener process [33][13][46], which is the integration of a white Gaussian random process. Although Wiener PHN $\theta(t)$ is

nonstationary, the LO output $e^{j\theta(t)}$ can be assumed stationary with a Lorentzian spectrum [33][13]. For Wiener PHN $\theta(t)$:

$$E[\theta(\tau)] = 0, \quad E[\theta(\tau_1)\theta(\tau_2)] = 4\pi\beta \min(\tau_1, \tau_2), \tag{5}$$

where β is the one-sided 3 dB bandwidth (unit Hz) of the Lorentzian spectrum. Discrete-time Wiener PHN can be expressed as $\theta[n+1] = \theta[n] + w_\theta[n]$ where $w_\theta[n]$ is zero-mean white Gaussian with variance σ_θ^2. σ_θ^2 and β are related by $\sigma_\theta^2 = 4\pi\beta T$, where T is the sampling period.

In the literature, $e^{j\theta(t)}$, $\theta(t)$, and $\phi(t)$ have been called PHN interchangeably, which may easily cause confusion. For clarity, we differentiate the three by naming $e^{j\theta(t)}$ the LO output, $\theta(t)$ the Wiener PHN, and $\phi(t)$ the stationary PHN, respectively.

It is noted that practical oscillator phase noise might be different from or more complex than the two described mathematical PHN models. Stationary PHN and Wiener PHN are used in this work to demonstrate the effectiveness of the proposed approach. This does not limit the proposed approach's applicability to other types of PHN. As demonstrated in the lab testing results, the proposed approach works for the PHN collected from a practical oscillator.

Chapter 3

Receiver Structure Overview

Conventional PHN compensation schemes estimate the PHN based on the received signal alone. In contrast, the proposed PHN compensation scheme employs an additional signal path from the oscillator to provide more information about the PHN, and as a result improves the PHN estimation.

3.1 The Conventional Receiver Architecture

Figure 5 shows a typical architecture of a conventional digital receiver equipped with PHN compensation capability, similar to that described in [29] and [16]. The LO output is $e^{-j[\omega_o t-\theta(t)]}$, where ω_o is the carrier frequency in radians. The received passband signal in complex form is $r(t)e^{j\omega_o t}$, where the baseband received signal $r(t)$ is

$$r(t)=\sum_k a_k g(t-kT)+w_1(t)\,. \tag{6}$$

In (6), a_k is the complex data symbol, $g(t)$ is the convolution of the transmitter pulse with the channel response, T is the symbol period, and $w_1(t)$ is the baseband complex white Gaussian noise with spectral density N_o. In the front-end, the mixture of the received passband signal with the LO output is followed by a low pass filter F(ω) (assumed to be an ideal brickwall lowpass filter) to produce the baseband signal

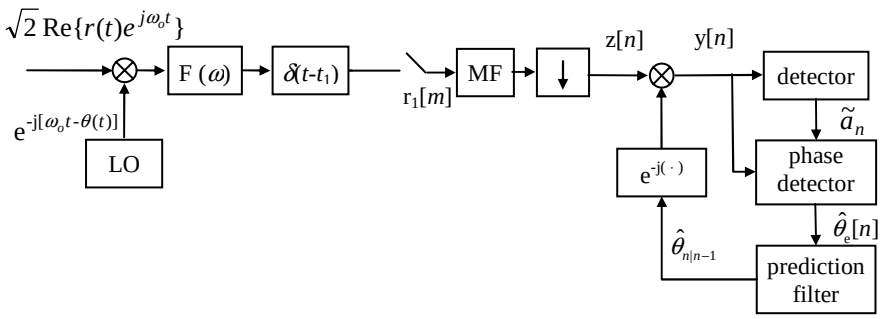

Figure 5. The conventional receiver model.

modulated by the PHN. The analogue delay $\delta(t\text{-}t_1)$ in Figure 5 explicitly models the inherent circuit delay associated with the analog front-end. This delay is included so as to be consistent with the proposed scheme where its effect can not be ignored. After sampling at the sampling rate $1/T_s$ which is higher than $1/T$, the baseband signal in Path I is:

$$r_1[m] \triangleq r(mT_s - t_1)e^{j\theta(mT_s - t_1)}. \tag{7}$$

To keep the analysis simple, T/T_s is assumed to be an integer. $r_1[m]$ is then fed into a digital pulse matched filter (MF). Assuming that symbol timing is achieved, which is a common assumption when phase recovery is considered [29], the MF output is decimated to the symbol rate T. The resulting signal is

$$\begin{aligned} z[n] &= \sum_m r_1[m] g_{MF}(nT - mT_s + t_1) \\ &= \sum_m r(mT_s - t_1) g_{MF}(nT - mT_s + t_1) e^{j\theta(mT_s - t_1)}, \end{aligned} \tag{8}$$

where $g_{MF}(t) = g(-t)$ is the impulse response of the MF. The difference in the time index used in (7) and (8) should be stressed. Herein, index n is used for the dis-

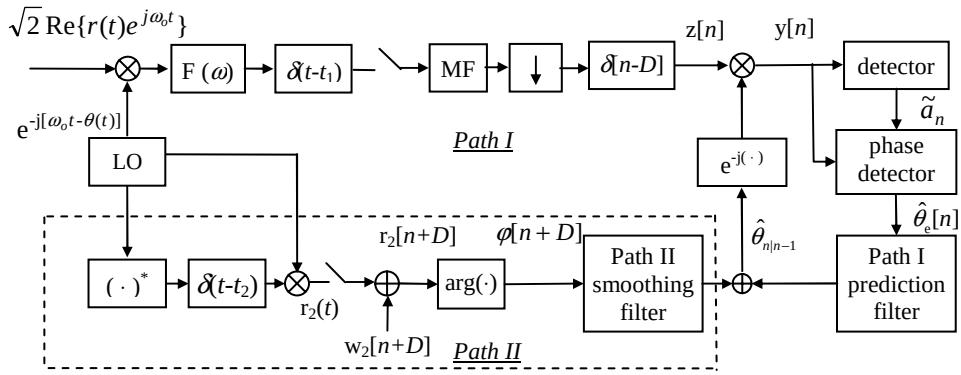

Figure 6. The proposed receiver model.

crete-time index at the MF output, which is at the symbol rate, while index m for the discrete-time index before the MF, which is at the sampling rate. PHN is compensated by multiplying $z[n]$ with the compensator $e^{-j\hat{\theta}_{n|n-1}}$ where $\hat{\theta}_{n|n-1}$ is the PHN estimate, as discussed in Chapter 4. The compensated signal

$$y[n] = z[n]e^{-j\hat{\theta}_{n|n-1}} \tag{9}$$

is used for data detection and phase error estimation.

3.2 The Proposed Receiver Architecture

Figure 6 shows an overview of the proposed digital receiver architecture for PHN compensation. Two signal flow paths can be recognized in Figure 6, i.e., the received signal path in the top (similar to the conventional scheme except for the delay block $\delta[n-D]$), and the additional path (in the dotted block) added to enhance the LO PHN estimation. For simplicity, these two paths will be referred to as Path I and Path II, respectively.

Path II is the key of this PHN compensation scheme. The motivation for adding this path is to observe a cleaner PHN without data modulation directly from the LO so as to obtain a better estimate of the PHN. The oscillator output is downconverted to the baseband by mixing itself with a delayed and conjugated replica. . This is readily implemented by employing an additional complex mixer and a delay element, both of which only add small additional area and power to an integrated analog front-end. Although the oscillator output can be directly sampled at a fraction of the carrier frequency to obtain the PHN information, such subsampling scheme would be overly sensitive to sampling jitter because of the high carrier frequency. The downconversion, therefore, is necessary in a practical system to reduce the sensitivity to sampling jitter. The mixer output is

$$r_2(t) = e^{j[\theta(t)-\theta(t-t_2)-\omega_0 t_2]} \triangleq e^{j[\theta(t)-\theta(t-t_2)+\gamma]}, \tag{10}$$

where t_2 is the delay added by the delay element as shown in Figure 6 and the constant $-\omega_0 t_2$ is denoted by γ. Because of the downconversion process, the observed signal in Path II is the difference of the PHN $\theta(t)$ and $\theta(t-t_2)$, instead of $\theta(t)$ itself. $r_2(t)$ is then sampled at symbol rate $1/T$:

$$r_2[n] \triangleq r_2(nT) = e^{j[\theta(nT)-\theta(nT-t_2)+\gamma]} + w_2[n], \tag{11}$$

where $w_2[n]$ is the additive white complex quantization noise, uniformly distributed with zero-mean and variance σ_{w2}^2. In Path II, quantization noise is the major noise source, and hence, it is modeled explicitly. The power of the quantization noise $w_2[n]$ depends on the bit resolution of the analog-to-digital converter (ADC). $\varphi[n]$,

the phase of $r_2[n]$, is applied to a smoothing filter $\mathbf{w}_2$, the output of which is combined with the PHN estimate from Path I to improve the overall phase estimate.

In the proposed scheme, Path I is similar to the conventional receiver, consisting of the analog front-end, data detection, and PHN prediction blocks. The primary difference from the conventional receivers is that a delay block $\delta[n-D]$ is added after the decimation operation. The reason for adding the delay block in Path I is so that future PHN information is available in Path II. For example, when data at time n is processed in Path I, PHN up to time $n+D$ is available in Path II. This will enable Path II to have access to future PHN information, and therefore estimate the PHN by a smoothing filter.

Chapter 4

Decision-Directed One-Step Phase Noise Estimation

Generally, the bandwidth of the LO output $e^{j\theta(t)}$ is much narrower than the bandwidth of the data signal and noise. Consequently, in the time domain, the PHN changes slowly compared to the data signal and noise, allowing us with little loss in accuracy to move the PHN term outside the convolution operation in (8). The resulting MF output becomes [43][29]

$$z[n] \approx \frac{E_g}{T_s} a_n e^{j\theta[n]} + w_g[n], \tag{12}$$

where a_n is the complex data symbol, $E_g \triangleq \int_{-\infty}^{\infty} g(t)g^*(t)dt$ is the energy contained in the pulse $g(t)$, $w_g[n] \triangleq \sum_m e^{j\theta(mT_s - t_1)} w(mT_s - t_1) g_{MF}(nT - mT_s + t_1)$ is the noise at the output of the MF, and

$$\theta[n] \triangleq \theta(\lfloor (nT + t_1)/T_s \rfloor T_s - t_1) \triangleq \theta(m_n T_s - t_1) = \theta(m_o T_s + nT - t_1) \tag{13}$$

is the effective PHN that affects symbol a_n. In (13), $\lfloor x \rfloor$ denotes the integer part of x. For simplicity, E_g / T_s in (12) is assumed to be 1 without loss in generality. The noise term $w_g[n]$ is zero-mean and approximately white Gaussian. The noise variance, $\sigma_{w_g}^2 = N_o / T_s$, is not altered by PHN, since the PHN does not change the

amplitude of the noise. It is noted that, in (12), $\theta[n]$ is the approximate PHN of the nth symbol, and the task of PHN estimation is to estimate $\theta[n]$.

Before introducing the proposed PHN estimation scheme, the conventional decision-directed one-step PHN estimation [10][29] is reviewed in Section 4.1. The proposed PHN estimation that employs signals from both paths is introduced in Section 4.2. The improvements of the proposed scheme are discussed in Section 4.3. Simulation results are provided in Section 4.4. Stationary PHN will be considered through Section 4.4, and Wiener PHN will be addressed in Section 4.5.

4.1 Conventional Decision-Directed One-Step Prediction Using Only Path I

The basic idea behind the decision-directed one-step PHN estimation is simple and consists of two steps. First, to estimate PHN $\theta[k]$, the estimate of the PHN $\theta[n]$ for $n < k$, $\hat{\theta}_{n|n}$, is calculated from the MF output $z[n]$ and past data a_n. In decision-directed approach, past data a_n are available from decision $\tilde{a}_n$. In another approach, namely the data-aided approach, past data a_n are known a priori from a pilot or training sequence. In our analysis, decisions are assumed to be correct: $\tilde{a}_n = a_n$ for $n < k$. In the second step, $\hat{\theta}_{n|n}$ for $n < k$ are used to estimate PHN $\theta[k]$, and the result of the one-step prediction of PHN $\theta[k]$ is denoted as $\hat{\theta}_{k|k-1}$. Herein, the subscript "$n|n$" is used for a filtered estimate of the PHN at time n using decisions

up to symbol n, and similarly, "$n|n-1$" for a prediction of the PHN at time n using decisions up to symbol n-1.

Write N_1 prior received signal $z[n]$ and decision $\tilde{a}_n$ in vector and matrix form, respectively:

$$\mathbf{z}_1 = [z[k-1], z[k-2], ..., z[k-N_1]]^T \tag{14}$$

$$\mathbf{A}_1 = diag\{\tilde{a}_{k-1}, \tilde{a}_{k-2}, \ldots, \tilde{a}_{k-N_1}\} = diag\{a_{k-1}, a_{k-2}, \ldots, a_{k-N_1}\}, \tag{15}$$

where the superscript 'T' stands for transpose and $diag\{\cdot\}$ stands for the diagonal matrix. Let R_w be the covariance matrix of the corresponding noise vector of $w_g[n]$ in (12), $k - N_1 \le n < k$. The maximum likelihood (ML) estimate of the phasor

$$\mathbf{e} = [e^{j\theta[k-1]}, e^{j\theta[k-2]}, ..., e^{j\theta[k-N_1]}]^T \tag{16}$$

can be obtained by [29]

$$\hat{\mathbf{e}} = (A_1^H R_w^{-1} A_1)^{-1} A_1^H R_w^{-1} \mathbf{z}_1, \tag{17}$$

where the superscript 'H' stands for Hermitian transpose. For Gaussian noise, the least square estimate, the best linear unbiased estimate, and the ML estimate share the same form as in (17). For white noise, (17) boils down to $\hat{\mathbf{e}} = A_1^{-1}\mathbf{z}_1$, which states that the ML estimate of the phasor $e^{j\theta[n]}$ is $z[n]/a[n]$. By the "invariant property" of the ML estimator [28],

$$\hat{\theta}_{n|n} = \arg(z[n]/a_n) \tag{18}$$

is the ML estimate of the phase $\theta[n]$ given the decision a_n. Applying (12) into (18) and defining $\xi_n \triangleq w_g[n]e^{-j\theta[n]}/a_n$, $\hat{\theta}_{n|n}$ can be approximated to the first order by:

$$\begin{aligned}\hat{\theta}_{n|n} &= \arg[e^{j\theta[n]}(1+\xi_n)] = \theta[n] + \arg[1+\xi_n] \\ &= \theta[n] + arctg\left[\frac{\mathrm{Im}\{\xi_n\}}{1+\mathrm{Re}\{\xi_n\}}\right] \\ &\approx \theta[n] + \mathrm{Im}[\xi_n](1-\mathrm{Re}[\xi_n]),\end{aligned} \tag{19}$$

where $|\xi_n| << 1$ is assumed. The assumption $|\xi_n| << 1$ means high SNR, which is the typical condition where PHN is problematic. For stationary PHN, plugging (1) into (13), $\theta[n]$ can be expressed as

$$\theta[n] = \theta_o + \phi(m_n T_s - t) \triangleq \theta_o + \phi[n], \tag{20}$$

Accordingly, $\hat{\theta}_{n|n}$ becomes

$$\hat{\theta}_{n|n} \approx \theta_o + \phi[n] + \mathrm{Im}[\xi_n](1-\mathrm{Re}[\xi_n]). \tag{21}$$

It can be shown that the zero-mean white noise $\mathrm{Im}[\xi_n](1-\mathrm{Re}[\xi_n])$ is uncorrelated to the stationary PHN $\phi[n]$.

In the one-step prediction, N_1 prior values of $\hat{\theta}_{n|n}$, represented in vector form as

$$\boldsymbol{\theta}_1 = [\hat{\theta}_{k-1|k-1}, \hat{\theta}_{k-2|k-2}, ..., \hat{\theta}_{k-N_1|k-N_1}]^T, \tag{22}$$

are used to predict the desired phase $\theta[k]$. Since $\boldsymbol{\theta}_1$ and $\theta[k]$ are not zero-mean, improved estimation can be achieved by employing the affine MMSE (AMMSE) estimator instead of the linear MMSE (LMMSE) estimator [21]. Assuming θ_o is known, which in practice requires a separate estimation device as described later, the AMMSE estimate of $\theta[k]$ using $\boldsymbol{\theta}_1$ (i.e., given data decisions of up to symbol a_{k-1}) is

$$\hat{\theta}_{k|k-1} = \mathbf{p}_1^T \mathbf{R}_1^{-1}(\boldsymbol{\theta}_1 - \theta_o \mathbf{e}_1) + \theta_o \tag{23}$$

where $\mathbf{R}_1$ is the auto-covariance matrix of $\boldsymbol{\theta}_1 - \theta_o \mathbf{e}_1$, $\mathbf{p}_1$ is the cross-covariance vector between $\boldsymbol{\theta}_1 - \theta_o \mathbf{e}_1$ and $\theta[k] - \theta_o$, and $\mathbf{e}_1$ is a vector of length N_1 with all elements being '1.' It is easy to show that the estimate $\hat{\theta}_{k|k-1}$ is unbiased. Defining the estimation error as

$$\theta_e[k] = \theta[k] - \hat{\theta}_{k|k-1}, \tag{24}$$

the error variance of the AMMSE estimation using one path is [21]:

$$\sigma_1^2 = E\left[\theta_e^2[k]\right] = \sigma_\phi^2 - \mathbf{p}_1^T \mathbf{R}_1^{-1} \mathbf{p}_1, \tag{25}$$

4.2 Proposed Joint Prediction and Smoothing PHN Estimation Using Both Paths

Path II provides additional PHN information from the oscillator. Unlike Path I, phase information in Path II does not suffer from data modulation. Therefore, the information in Path II can be used jointly with the PHN information in Path I to enhance the PHN estimate. Comparing (11) and (12), it is clear that signal in Path II has a similar form to that of Path I, except that signal in Path II can be viewed as being modulated with a data sequence of constant '1's. Moreover, as pointed in Section 3.2, Path II contains information of future PHN. Thus, unlike the decision-directed one-step prediction employed in Path I, information from Path II can be used in a data-aided smoothing manner.

The phase of the samples $r_2[n]$ in Path II can be approximated to first order as in (19). Defining $\varsigma_n = w_2[n] e^{-j\left(\theta(nT) - \theta(nT - t_2) + \gamma\right)}$ and assuming $\left|w_2[n]\right| << 1$, it follows that

$$\begin{aligned}\varphi[n] &= \arg\left[r_2[n]\right] = \arg\left[e^{j\left(\theta(nT)-\theta(nT-t_2)+\gamma\right)}\left(1+\varsigma_n\right)\right] \\ &\approx \theta(nT)-\theta(nT-t_2)+\gamma+\mathrm{Im}[\varsigma_n](1-\mathrm{Re}[\varsigma_n]).\end{aligned} \tag{26}$$

To estimate PHN $\theta[k]$, a smoothing filter is employed in Path II, using both past and future values of $\varphi[n]$. The observation vector, which consists of N_2 past values and D future values of $\varphi[n]$, can be represented as:

$$\boldsymbol{\theta}_2 = [\varphi[k+D],...,\varphi[k],...,\varphi[k-N_2]]^T . \tag{27}$$

Although it is possible to estimate $\theta[k]$ from $\boldsymbol{\theta}_2$, the performance is limited noting that the useful PHN information in Path II is the difference $\theta(nT)-\theta(nT-t_2)$ instead of the PHN $\theta(nT)$ itself. The amplitude of the frequency response of the difference operator $1-\delta(t-t_2)$ is $\sin\pi f t_2$, which is 0 at $f=k/t_2$ (k is any integer). This suggests that part of the PHN information is lost by this filter, especially those in the vicinity of the oscillation frequency. Therefore, it is more effective to augment the PHN estimation with Path II rather than to use Path II alone. It also shows that the value of the delay t_2 should be set carefully, as seen later in this chapter.

With the information from both Path I and Path II, we can form a combined centralized observation vector:

$$\boldsymbol{\theta} = [(\boldsymbol{\theta}_1-\theta_o\mathbf{e}_1)^T \quad (\boldsymbol{\theta}_2-\gamma\mathbf{e}_2)^T]^T , \tag{28}$$

where $\mathbf{e}_2$ is a vector of the same length as $\boldsymbol{\theta}_2$ and all elements being '1.' AMMSE is again employed to estimate $\theta[k]$ from $\boldsymbol{\theta}$:

$$\begin{aligned}\hat{\theta}_{k|k-1} &= \mathbf{p}^T\mathbf{R}^{-1}\boldsymbol{\theta}+\theta_o = \mathbf{w}_{opt}^T\boldsymbol{\theta}+\theta_o \\ &= \mathbf{w}_{opt1}^T(\boldsymbol{\theta}_1-\theta_o\mathbf{e}_1)+\mathbf{w}_{opt2}^T(\boldsymbol{\theta}_2-\gamma\mathbf{e}_2)+\theta_o.\end{aligned} \tag{29}$$

In (29), $\mathbf{R}$ is the covariance matrix of $\boldsymbol{\theta}$, $\mathbf{p}$ is the covariance vector between $\boldsymbol{\theta}$ and $\theta[k]-\theta_o$, and $\mathbf{w}_{opt}=\mathbf{p}^T\mathbf{R}^{-1}$ is divided into two subfilters, $\mathbf{w}_{opt1}$ and $\mathbf{w}_{opt2}$, corresponding to Path I and Path II respectively. The calculations of $\mathbf{R}_1$, $\mathbf{R}$, $\mathbf{p}_1$, and $\mathbf{p}$ in (23) and (29) are lengthy but straightforward, as shown in Appendix A.

Similar to (25), the error variance of the PHN estimate using both paths is

$$\sigma^2=\sigma_\phi^2-\mathbf{p}^T\mathbf{R}^{-1}\mathbf{p} \tag{30}$$

Since the joint AMMSE PHN estimation in (29) combines the prediction filter in Path I and the smoothing filter in Path II, it improves the estimation error performance significantly over PHN estimation using only Path I, as will be shown in Section 4.3.

There is a practical difficulty in obtaining $\hat{\theta}_{k|k}$ through (18) due to the 2π boundary problem of the function of $\arg[\cdot]$. To show this problem, the range of $\arg[\cdot]$ is assumed to be (-π,π]. When θ_o is close to π, for example, $\hat{\theta}_{k|k}$ obtained by (18) will fluctuate between values close to either π or -π due to PHN $\phi[n]$ and noise $\mathrm{Im}[\xi_n](1-\mathrm{Re}[\xi_n])$, making (19) invalid. Based on the relation between $z[k]$ and $y[k]$ as shown in (9), the estimate of the estimation error $\theta_e[k]$ can be obtained by

$$\begin{aligned}\hat{\theta}_e[k]&=\arg(y[k]/\tilde{a}_k)=\arg(z[k]e^{-j\hat{\theta}_{k|k-1}}/\tilde{a}_k)\\&\approx\theta[k]-\hat{\theta}_{k|k-1}+\mathrm{Im}[\xi_k](1-\mathrm{Re}[\xi_k])\\&=\theta_e[k]+\mathrm{Im}[\xi_k](1-\mathrm{Re}[\xi_k])\end{aligned} \tag{31}$$

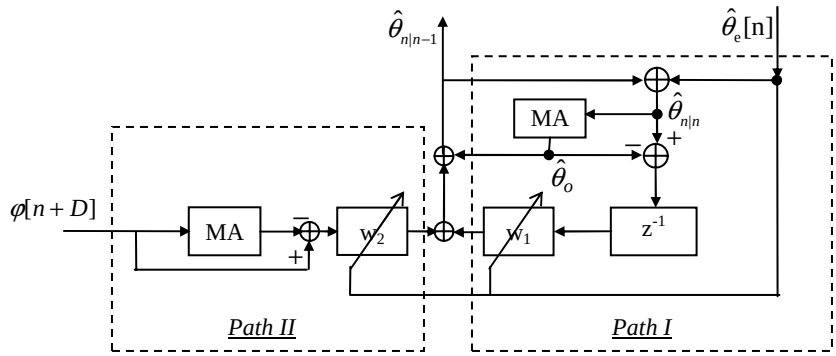

(c)

Figure 7. The PHN estimation block.

The operator $\arg(y[k]/\tilde{a}_k)$ in (31) serves as the phase detector in Figure 6. Since $\theta_e[k]$ is a small value around 0, phase detector $\arg(y[k]/\tilde{a}_k)$ can circumvent the 2π boundary problem that might arise when using (18) directly. With $\hat{\theta}_e[k]$ available, $\hat{\theta}_{k|k}$ can be found by

$$\hat{\theta}_{k|k} = \hat{\theta}_e[k] + \hat{\theta}_{k|k-1}, \tag{32}$$

which can be confirmed by adding the noise term $\mathrm{Im}[\xi_n](1-\mathrm{Re}[\xi_n])$ to both sides of (24) and plugging the result into (21).

In practice, θ_o is generally unknown and can be obtained using a phase tracking device [10][29]. A moving average (MA) filter operating on $\hat{\theta}_{n|n}$ can also be used to estimate θ_o. Parameter γ in Path II is obtained in a similar manner using a MA filter. Figure 7 shows the structure of the joint PHN estimation using both Path I and Path II, in which the filter with taps $\mathbf{w}_1$ is the Path I prediction filter and the filter with taps $\mathbf{w}_2$ is the Path II smoothing filter.

Although error variance is a direct measure of the PHN estimation, it is helpful to know the SNR after the PHN compensation to evaluate the system performance. From (9) and (12), the MF output after PHN compensation is

$$\begin{aligned} y[n] &= a_n e^{j\theta_e[n]} + w_g[n] e^{-j\hat{\theta}_{n|n-1}} \\ &\approx a_n + j\theta_e[n] a_n + w_g[n] e^{-j\hat{\theta}_{n|n-1}} \end{aligned}, \tag{33}$$

Therefore, the compensated SNR after PHN compensation without and with Path II are respectively

$$\begin{aligned} SNR_1 &= \frac{E[|a_n|^2]}{E[|a_n|^2]E[|\theta_e[n]|^2] + E[|w_g[n]e^{j\theta_{n|n-1}}|^2]} \\ &= \frac{1}{\sigma_1^2 + \sigma_{w_g}^2 \big/ E[|a_n|^2]} \\ &= \frac{1}{\sigma_1^2 + 1/SNR_{in1}} \end{aligned} \tag{34}$$

and

$$\begin{aligned} SNR &= \frac{1}{\sigma^2 + \sigma_{w_g}^2 \big/ E[|a_n|^2]} \\ &= \frac{1}{\sigma^2 + 1/SNR_{in1}} \end{aligned}, \tag{35}$$

where $\sigma_{w_g}^2$ is the variance of $w_g[n]$ in (12), and $SNR_{in1} = E[|a_n|^2] \big/ \sigma_{w_g}^2$ is the input symbol SNR at the MF output in the absence of PHN, representing the signal to white Gaussian noise ratio.

4.3 Improvement in Phase Noise Compensation Capability

Since Path II provides extra and future information of PHN directly from the oscillator, the proposed scheme is expected to provide a better PHN estimate than the

conventional estimate based on Path I only. This advantage can be easily confirmed by comparing the variance of the remaining phase error without and with Path II, given by (25) and (30), respectively. For joint PHN estimation in (29), $\mathbf{R}$ can be divided into subblocks

$$\mathbf{R} = \begin{pmatrix} \mathbf{R}_1 & \mathbf{R}_{12} \\ \mathbf{R}_{12}^T & \mathbf{R}_2 \end{pmatrix}, \tag{36}$$

in which $\mathbf{R}_1$ is the same as in (23), $\mathbf{R}_{12}$ is the cross-covariance between $\boldsymbol{\theta}_1 - \theta_o \mathbf{e}_1$ and $\boldsymbol{\theta}_2 - \gamma \mathbf{e}_2$, and $\mathbf{R}_2$ is the auto-covariance matrix of $\boldsymbol{\theta}_2 - \gamma \mathbf{e}_2$. $\mathbf{p}$ can also be divided into two subvectors, $\mathbf{p}_1$ and $\mathbf{p}_2$, corresponding to Path I and Path II respectively,

$$\mathbf{p} = [\mathbf{p}_1^T \quad \mathbf{p}_2^T]^T, \tag{37}$$

where $\mathbf{p}_1$ is the same as in (23). Applying the partitioned matrix inverse formula [21] to (36), the second term on the right side of (30) becomes

$$\mathbf{p}^T \mathbf{R}^{-1} \mathbf{p} = \mathbf{p}_1^T \mathbf{R}_1^{-1} \mathbf{p}_1 + \mathbf{p}^T \begin{pmatrix} -\mathbf{R}_1^{-1}\mathbf{R}_{12} \\ \mathbf{I} \end{pmatrix} \left(\mathbf{R}_2 - \mathbf{R}_{12}^T \mathbf{R}_1^{-1} \mathbf{R}_{12} \right)^{-1} \begin{pmatrix} -\mathbf{R}_{12}^T \mathbf{R}_1^{-1} & \mathbf{I} \end{pmatrix} \mathbf{p}. \tag{38}$$

The matrix $\left(\mathbf{R}_2 - \mathbf{R}_{12}^T \mathbf{R}_1^{-1} \mathbf{R}_{12} \right)$ in the second term on the right-hand side of (38) is positive-definite, and so is its inverse. This can be easily shown by recognizing that $\left(\mathbf{R}_2 - \mathbf{R}_{12}^T \mathbf{R}_1^{-1} \mathbf{R}_{12} \right)$ is the error covariance of estimating $\boldsymbol{\theta}_2 - \gamma \mathbf{e}_2$ from $\boldsymbol{\theta}_1 - \theta_o \mathbf{e}_1$ using a Wiener filter. Consequently, $\mathbf{p}^T \mathbf{R}^{-1} \mathbf{p} > \mathbf{p}_1^T \mathbf{R}_1^{-1} \mathbf{p}_1$ and

$$\sigma^2 = \sigma_\phi^2 - \mathbf{p}^T \mathbf{R}^{-1} \mathbf{p} < \sigma_\phi^2 - \mathbf{p}_1^T \mathbf{R}_1^{-1} \mathbf{p}_1 = \sigma_1^2. \tag{39}$$

(39) is consistent with the intuition that the additional information provided by Path II should only help if properly used.

In practice, the oscillators at the transmitters also contribute to the PHN in the received signal. It should be pointed out that the proposed scheme improves the compensation of the PHN introduced at the receiver, while maintaining the same compensation capability as conventional schemes for PHN introduced at the transmitters. For PHN from the transmitters, this can be readily shown from (38): the independence of the PHN in the transmitter and receiver causes all components of $\mathbf{p}_2$ and $\mathbf{R}_{12}$, corresponding to the covariance between the transmitter and receiver PHN, to be zero. The idea of using an additional signal path to compensate PHN can also be extended to the transmitter, as shown in later chapters.

4.4 Simulation Results

To illustrate the benefits of Path II, numerical performance results for a 64-QAM system are presented. The symbol period T is assumed to be 10^{-6}s, and the sampling period $T_s=T/2$. AWGN channel is assumed, and the input SNR in Path I SNR_{in1} is set to 29 dB. 29 dB is chosen as a relative high input SNR value at which PHN dominates the performance. In Path II, the major source of noise is the quantization noise due to the ADC. The SNR in Path II, which is defined as $SNR_{in2} = 1/\sigma_{w2}^2$, is 37.88 dB, corresponding to an ADC of 6 bits. The delay associated with Path I, t_1, is set to $0.25T$. There are N_1=8 filter taps in Path I prediction filter, and 11 taps in Path II smoothing filter, of which N_2=8 taps in Path II correspond to the 'past' ($\varphi[k-1],...,\varphi[k-N_2]$ in (27)), and D=2 taps in Path II to the 'future' ($\varphi[k+D],...,\varphi[k+1]$ in (27)).

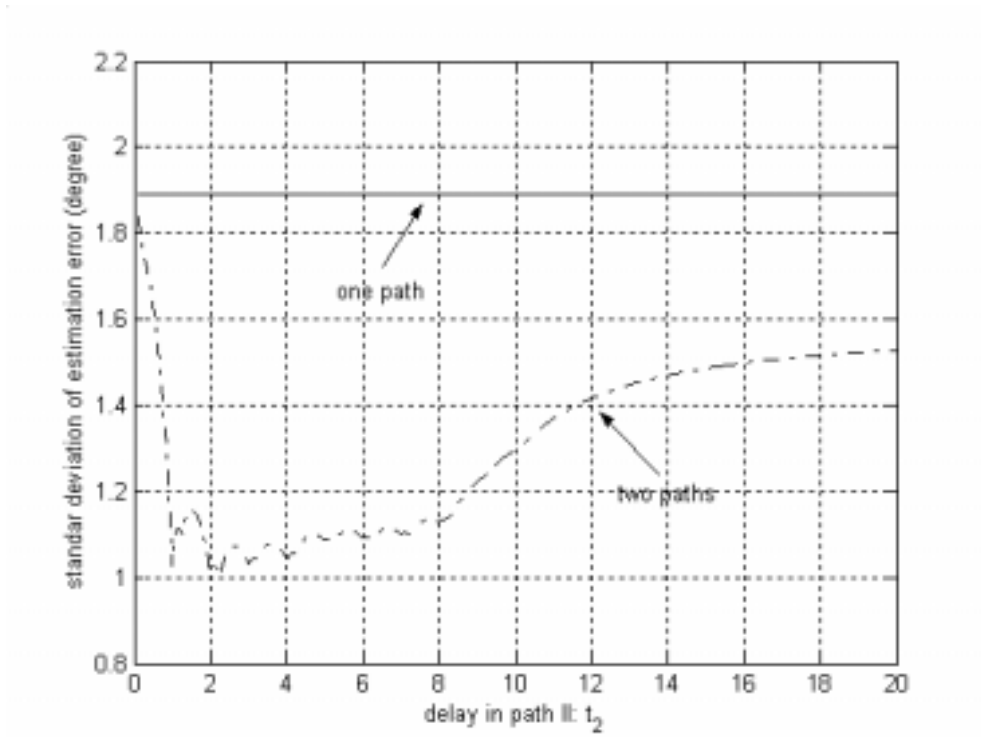

Figure 8. Standard deviation of PHN estimation error variance vs. t_2.

The relation between PHN estimation error and the delay in Path II, t_2, is depicted in Figure 8, in which PHN is stationary with $\sigma_\phi^2 = 0.0076$ (standard deviation $\sigma_\phi = 5^0$), and the 3 dB bandwidth B_ϕ =5 kHz. The horizontal axis is normalized by symbol period T, and changes from 0.01T to 20T. The proposed scheme reduces the standard deviation of estimation error from 1.9^o to 1°, which translates into a 1.7 dB improvement in compensated SNR. The performance curve has several local minima, which occur when t_2 or $t_2 - t_1$ is a multiple of T.

From Figure 8, it can be observed that the range of the "high" performance region for t_2 is from approximately T to N_1T. This can be understood heuristically by observing the relationship of Path I observation $\theta[n]$ and Path II observation $\varphi[n]$ in

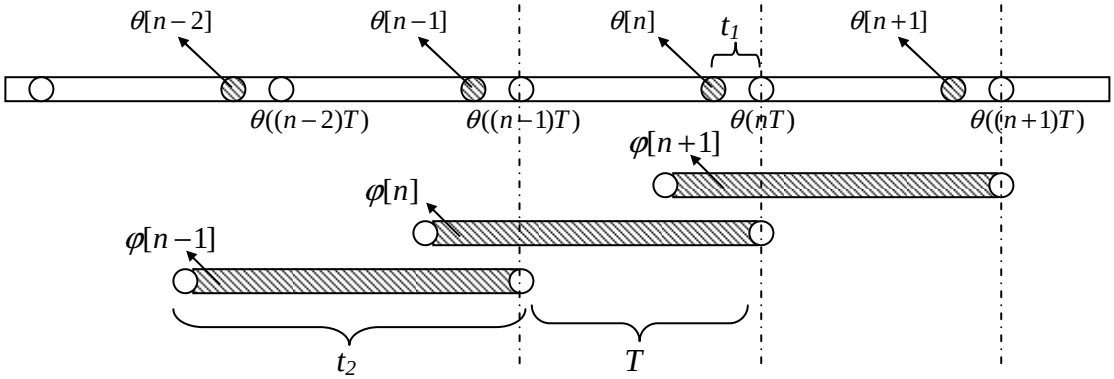

Figure 9. Relationship of Path I observation $\theta[n]$ and Path II observation $\varphi[n]$ in time.

time, as shown in Figure 9. The observations from Path II provide the increment in PHN while those from Path I provide some "starting points" or "base points" for estimation. When t_2 is so large that the starting points of $\varphi[n]$ is out of the range of the Path I observation vector $\boldsymbol{\theta}_1$, the PHN estimation performance begins to drop. Meanwhile, if t_2 is very small, the observation from Path II can not provide enough PHN increment information, which again will degrade the PHN estimation performance. When $t_2 - t_1$ or t_2 is a multiple of T, the starting point of $\varphi[n]$ will align with $\theta[n]$ or the end point of $\varphi[n-1]$, which will provide exact PHN increment information and therefore improve PHN estimation.

Figure 10 plots the standard deviation of the remaining PHN and the SNR after compensation as a function of the standard deviation of the PHN. The delay in Path II is fixed at t_2=1.25T for high performance as discussed above. The standard

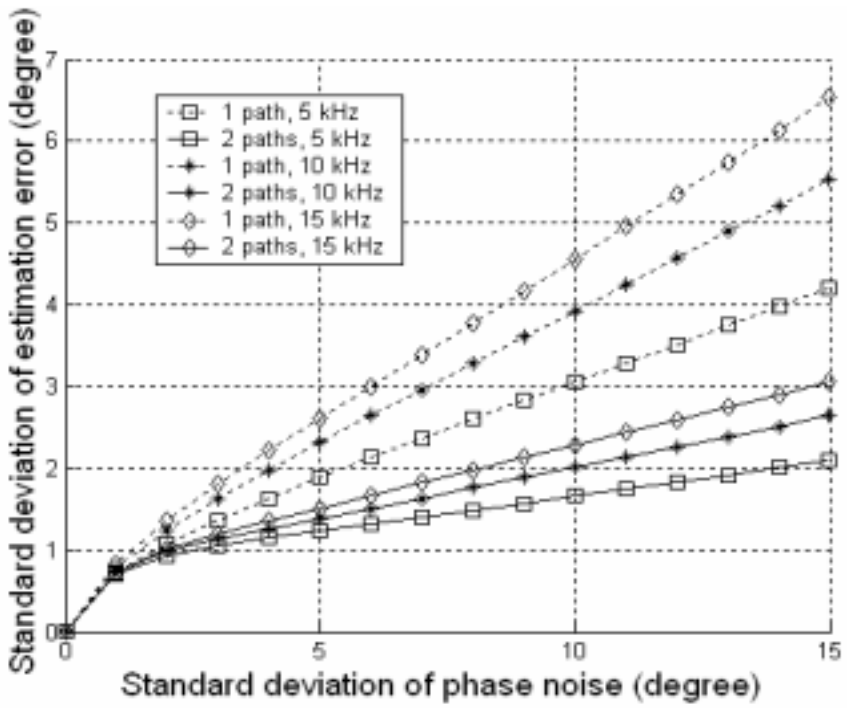

(a)

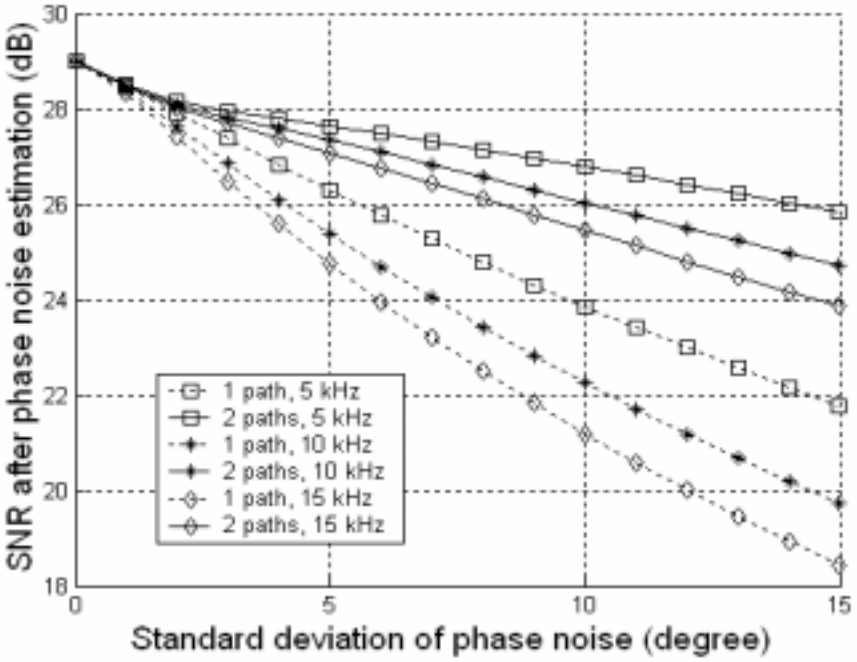

(b)

Figure 10. PHN Standard deviation (a) and SNR (b) after PHN compensation vs. standard deviation of PHN for stationary PHN.

deviation of the PHN changes from 0 to 15°, and the PHN bandwidth is set to 5 kHz, 10 kHz, and 15 kHz, respectively. The improvement in SNR after compensation can be as high as 5.4 dB at $\sigma_\phi = 15^o$. Figure 10 suggests that the proposed scheme can combat heavy phase noise effectively. Therefore, a less stringent requirement on the front-end oscillator design becomes possible.

Figure 11 depicts the standard deviation of the remaining PHN and the compensated SNR vs. SNR_{in1}, the input SNR for Path I. SNR_{in1} varies from 25 to 35 dB. The standard deviation (in degree) and bandwidth of PHN are set to be 2° and 2 kHz, 5° and 5 kHz, and 10° and 10 kHz, respectively. Figure 11 also shows that the proposed scheme is less sensitive to PHN. For example, the two path performance at 5° and 5k Hz is close to the one path performance at 2° and 2k, while the two path performance at 10° and 10k Hz is close to the one path performance at 5° and 5k Hz.

The input SNR in Path II, SNR_{in2}, also plays a role in the performance by affecting **R** in (30). Since the complex uniform distributed quantization noise is the dominant noise source in Path II, the choice of the number of bits of Path II ADC, N_{ADC}, dictates SNR_{in2}:

$$SNR_{in2} = \frac{1}{\sigma_{w2}^2} = \frac{1}{2\frac{(\frac{2}{2^{N_{ADC}}})^2}{12}} = 3 \cdot 2^{2N_{ADC}-1} \tag{40}$$

Although a large N_{ADC} improves SNR_{in2}, the complexity of Path II increases. Figure 12 plots the compensated SNR vs. N_{ADC}, where the PHN bandwidth is set to 5 kHz, and the standard deviation of PHN is set to 5°, 10°, and 15°, respectively. From

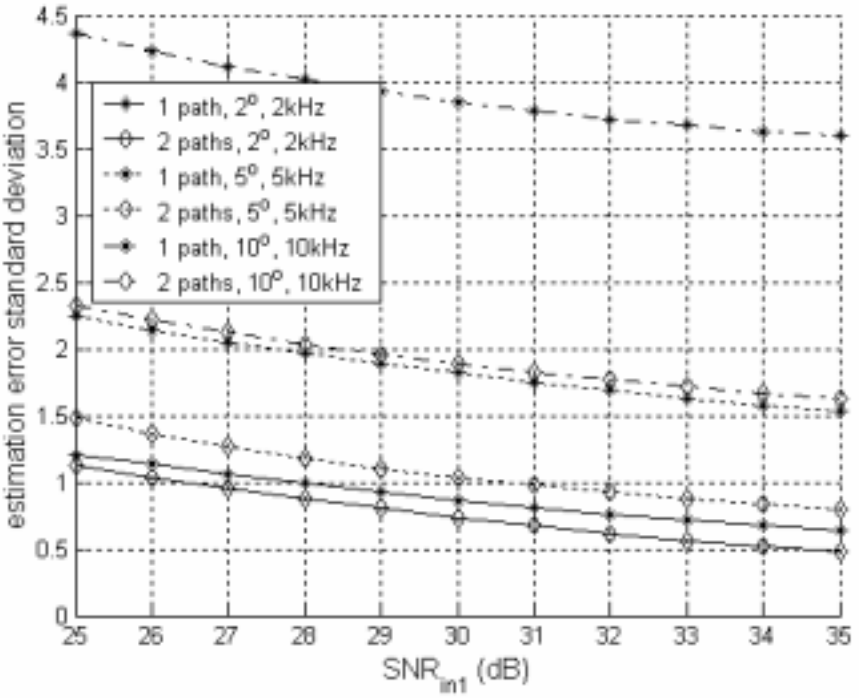

(a)

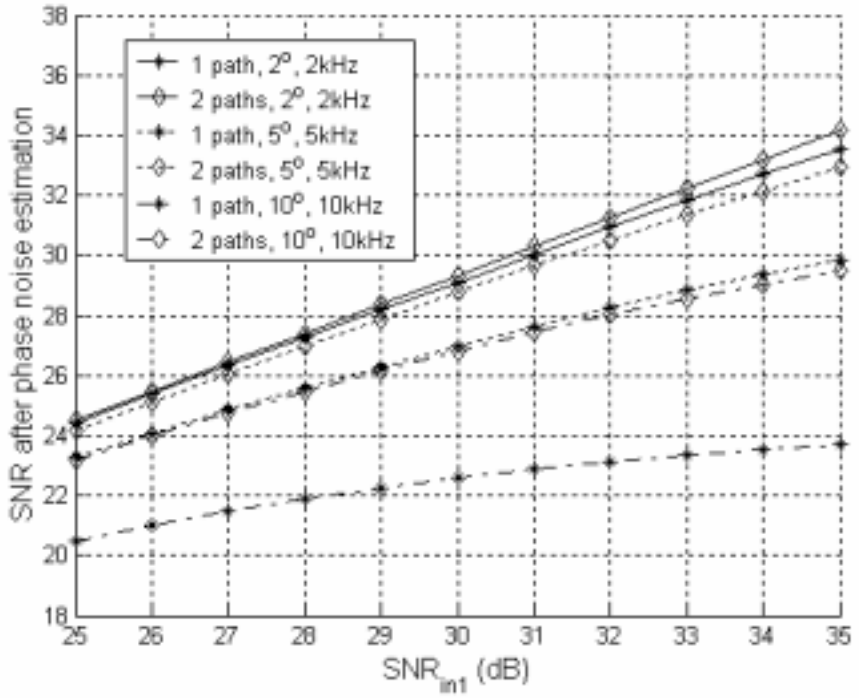

(b)

Figure 11. PHN standard deviation (a) and SNR (b) after PHN compensation vs. SNR_{in1}

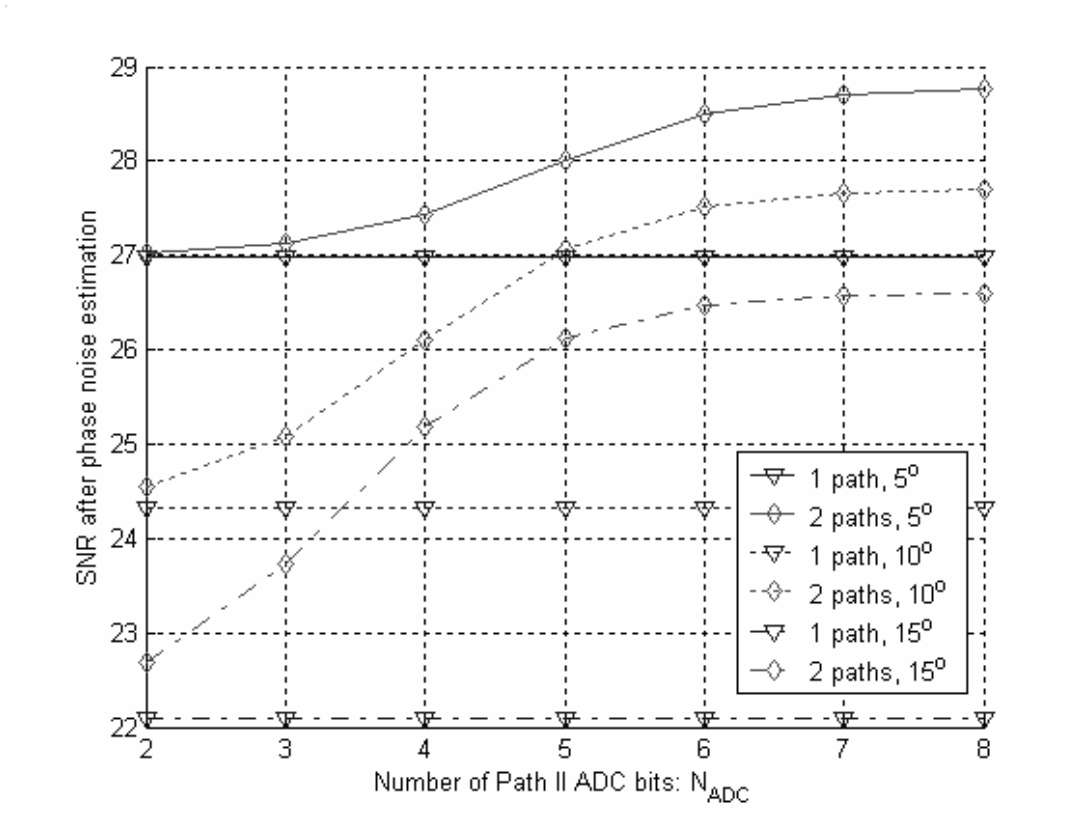

Figure 12 Compensated SNR vs. number of bits in Path II ADC.

Figure 12, it can be observed that 6 bits (SNR_{in2}=37.88 dB) is adequate for Path II ADC as the performance saturates for higher bits.

4.5 Wiener Phase Noise Estimation

The "2-Paths" structure in Figure 6 can combat Wiener PHN effectively as well, although Wiener PHN is nonstationary and its statistical properties are different from stationary PHN. As in the decision-directed estimation of the stationary PHN, past data decisions $\tilde{a}_n$ ($n < k$) are assumed to be correct to obtain $\hat{\theta}_{n|n}$. Past values of the filtering PHN estimate $\hat{\theta}_{n|n}$ from Path I and the Path II observations are then used

to estimate $\hat{\theta}_{k|k-1}$ jointly. For Wiener PHN, $\hat{\theta}_{k-i|k-i}\,(1 \le i \le N_1)$ is non-stationary and the variance goes unbounded when k becomes large, which is clear from (5). This problem can be overcome by centralizing the past values of the filtering PHN estimate $\hat{\theta}_{n|n}$, i.e. subtracting the mean of past values from $\hat{\theta}_{n|n}$.

Define the average of N prior values of $\hat{\theta}_{k-i|k-i}$ as

$$\theta_o[k] = \frac{1}{N}\sum_{l=1}^{N}\hat{\theta}_{k-l|k-l}\,, \tag{41}$$

where N is the length of the moving average filter. The centralized value $\hat{\theta}_{k-i|k-i} - \theta_o[k]$ has the same second-order statistical properties for every k. Represented in vector form, N_1 prior values of the centralized $\hat{\theta}_{k-i|k-i}$ form the observation in Path I:

$$\mathbf{\theta}_1 = [\hat{\theta}_{k-1|k-1}, \hat{\theta}_{k-2|k-2}, ..., \hat{\theta}_{k-N_1|k-N_1}]^T - \theta_o[k]\mathbf{e}_1 \tag{42}$$

Note that $\mathbf{\theta}_1$ in (22) and (42) are different. In this section, some terms are redefined for Wiener PHN. Using the properties of Wiener PHN, the $(i, j)^{\text{th}}$ element of the correlation matrix of $\mathbf{\theta}_1$ for Wiener PHN can be shown to be

$$\begin{aligned}\mathbf{R}_1(i,j) &= \sigma_\theta^2[(N+1)(2N+1)/(6N) + (i^2+i+j^2+j)/(2N) - \max(i,j)] \\ &+ \left(\delta(i-j) - \frac{1}{N}\right)\left(\frac{1}{2}\sigma_{w_g}^2 E[\frac{1}{|a_n|^2}] + \frac{1}{4}\sigma_{w_g}^4 E[\frac{1}{|a_n|^4}]\right)\end{aligned} \quad . \tag{43}$$

To avoid an ill-conditioned $\mathbf{R}_1$, N is chosen to be slightly larger than N_1. The ith element of the correlation vector between $\mathbf{\theta}_1$ and $\theta[k] - \theta_o[k]$ for Wiener PHN is

$$\mathbf{p}_1(i) = \sigma_\theta^2[(N+1)(2N+1)/(6N) + (i^2 - i)/(2N) - i]\,. \tag{44}$$

It is clear from (43) and (44) that $\mathbf{R}_1$ and $\mathbf{p}_1$ for the centralized Wiener PHN does not change over time. Therefore, Wiener filter can be formed to predict $\theta[k]-\theta_o[k]$ from $\boldsymbol{\theta}_1$, and $\hat{\theta}_{k|k-1}$ is given by

$$\hat{\theta}_{k|k-1} = \mathbf{p}_1^T \mathbf{R}_1^{-1} \boldsymbol{\theta}_1 + \theta_o[k]. \tag{45}$$

The variance of the prediction error $\theta_e[k]$ using (45) is given by

$$\begin{aligned} \sigma_1^2 &= E\left[\theta_e^2[k]\right] = E\left[\left(\theta[k]-\theta_o[k]\right)^2\right] - \mathbf{p}_1^T \mathbf{R}_1^{-1} \mathbf{p}_1 \\ &= \frac{(N+1)(2N+1)}{6N}\sigma_\theta^2 + \frac{1}{N}\left(\frac{1}{2}\sigma_{w_g}^2 E[\frac{1}{|a_n|^2}] + \frac{1}{4}\sigma_{w_g}^4 E[\frac{1}{|a_n|^4}]\right) - \mathbf{p}_1^T \mathbf{R}_1^{-1} \mathbf{p}_1 \end{aligned} \tag{46}$$

It is noted that the Kalman filter can also be used to estimate Wiener PHN, which is a first-order Gauss-Markov process. The performance of the Kalman filter, however, can be shown to be comparable to that of the Wiener filter. This proposal therefore focuses on the use of the Wiener filter for its simplicity.

In Path II, the observations $\varphi[n]$ has the same form as (26), because, unlike $\hat{\theta}_{n|n}$ in Path I, $\varphi[n]$ is stationary since $\theta(nT)-\theta(nT-t_2)$ is zero-mean and stationary. Having the mean value removed, Path II observations can be expressed in vector form:

$$\boldsymbol{\theta}_2 = [\varphi[k+D],...,\varphi[k],...,\varphi[k-N_2]]^T - \gamma \mathbf{e}_2 \tag{47}$$

The AMMSE estimate of $\theta[k]$ based on observations $\boldsymbol{\theta} = [\boldsymbol{\theta}_1{}^T \quad \boldsymbol{\theta}_2{}^T]^T$ from both Path I and Path II is given by

$$\hat{\theta}_{k|k-1} = \mathbf{p}^T \mathbf{R}^{-1} \boldsymbol{\theta} + \theta_o[k] \triangleq \mathbf{w}_{opt1}^T \boldsymbol{\theta}_1 + \mathbf{w}_{opt2}^T \boldsymbol{\theta}_2 + \theta_o[k]. \tag{48}$$

In (48), $\mathbf{R}$ is the correlation matrix of $\boldsymbol{\theta}$, $\mathbf{p}$ is the correlation vector between $\boldsymbol{\theta}$ and $\hat{\theta}_{k-i|k-i} - \theta_o[k]$. The calculations of $\mathbf{R}$ and $\mathbf{p}$ can be obtained by making use of the properties of Wiener PHN (5), and the calculation details are provided in Appendix B, where it is shown that, similar to $\mathbf{R}_1$ and $\mathbf{p}_1$, $\mathbf{R}$ and $\mathbf{p}$ are time-invariant.

The optimal filter is divided into two subfilters, $\mathbf{w}_{opt1}$ and $\mathbf{w}_{opt2}$, corresponding to Path I and Path II respectively, similar to that for stationary PHN. The structure of Wiener PHN estimation is similar to that of stationary PHN estimation shown in Figure 7, except that the length of the moving average filter is much shorter than that of stationary PHN. The length of the moving average filter can be left as a parameter to choose during implementation. The error variance of the joint prediction-smoothing estimate of the Wiener PHN is given by

$$\begin{aligned}\sigma^2 &= E\left[\left(\theta[k]-\theta_o[k]\right)^2\right] - \mathbf{p}^T\mathbf{R}^{-1}\mathbf{p} \\ &= \frac{(N+1)(2N+1)}{6N}\sigma_\theta^2 + \frac{1}{N}\left(\frac{1}{2}\sigma_{w1}^2 E[\frac{1}{|a_n|^2}] + \frac{1}{4}\sigma_{w1}^4 E[\frac{1}{|a_n|^4}]\right) - \mathbf{p}^T\mathbf{R}^{-1}\mathbf{p}\end{aligned} \tag{49}$$

With the estimation error variance for Wiener PHN established, the SNR after PHN compensation can be evaluated by (34) and (35), respectively.

To illustrate the effectiveness of employing Path II to compensate Wiener PHN, numerical performance results for a 64-QAM system are presented. The system settings are the same as that for stationary PHN except that PHN herein is Wiener PHN. The length of the moving average in Path I is N=20. Figure 13 depicts the SNR after compensation vs. the standard deviation of the Wiener PHN increment σ_θ, from which significant improvement can be observed.

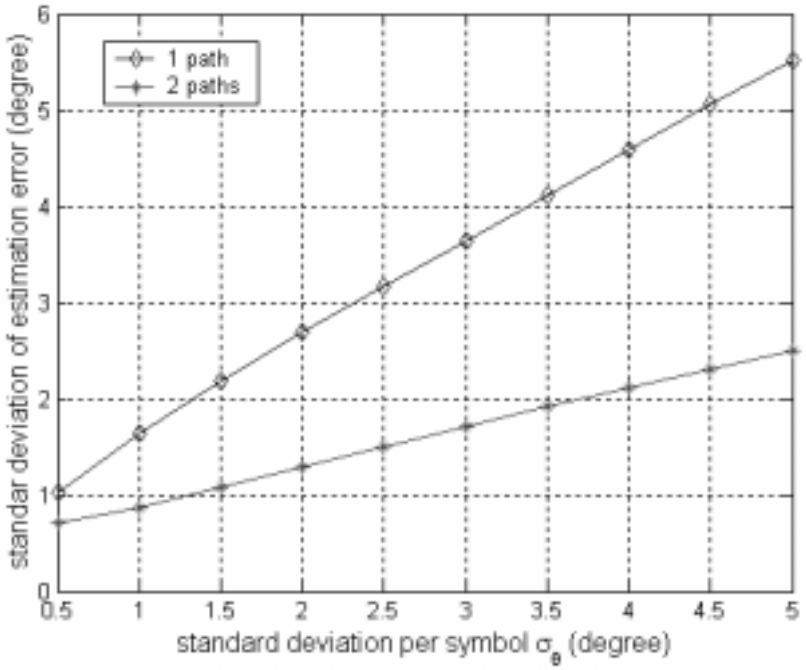

(a)

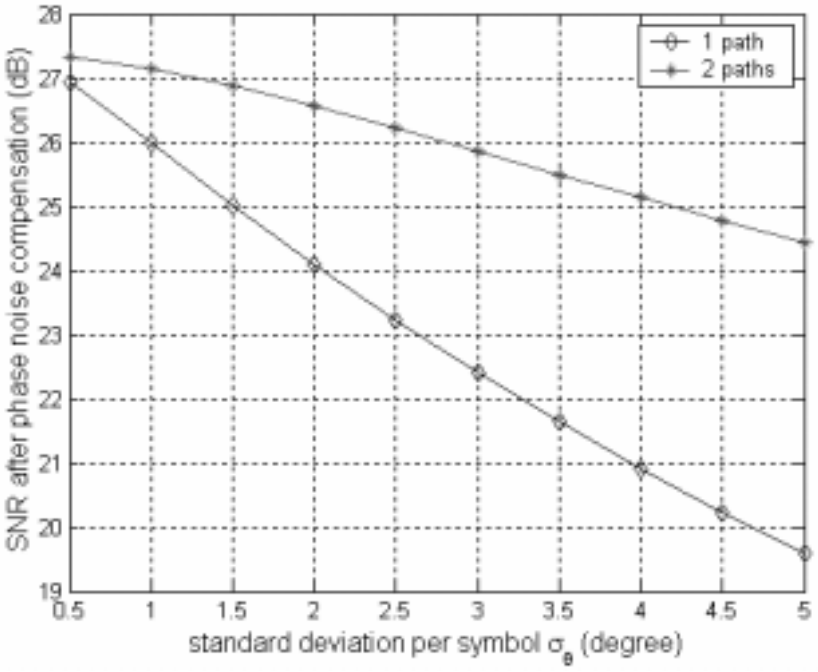

(b)

Figure 13. Remaining PHN standard deviation and SNR after PHN compensation vs. standard deviation

Chapter 5

Adaptive Algorithms and Lab Testing Results

5.1 Adaptive PHN Estimation

The phase noise needs to be adaptively estimated for several reasons. Most often, the statistical properties needed to calculate the optimum weights, as shown in Chapter 4, are not available or hard to obtain. In addition, those phase noise properties may change due to variations in the operating conditions. To adaptively adjust the weights to the optimal values and track the time variations, adaptive algorithms can be employed, such as the least-mean-square (LMS) algorithm or the recursive-least-square (RLS) algorithm [20].

The LMS algorithm adapts the weights by:

$$\mathbf{w}_{k+1} = \mathbf{w}_k + \mu \boldsymbol{\theta}_k \theta_e[k] = \mathbf{w}_k + \mu \boldsymbol{\theta}_k (\theta[k] - \hat{\theta}_{k|k-1}), \tag{50}$$

where the subscript k denotes the kth step, and μ is the step size parameter. The step sizes for filters in Path I and Path II can be made different to accommodate the different filter input power.

The RLS algorithm adapts the weights by

$$\mathbf{w}_k = \mathbf{w}_{k-1} + \mathbf{P}_k \boldsymbol{\theta}_k (\theta[k] - \hat{\theta}_{k|k-1})$$

$$\mathbf{P}_k = \lambda^{-1} \left(\mathbf{P}_{k-1} - \frac{\lambda^{-1} \mathbf{P}_{k-1} \boldsymbol{\theta}_k^T \boldsymbol{\theta}_k \mathbf{P}_{k-1}}{1 + \lambda^{-1} \boldsymbol{\theta}_k^T \mathbf{P}_{k-1} \boldsymbol{\theta}_k} \right) \tag{51}$$

with initial condition $\mathbf{P}_0 = \varepsilon^{-1}\mathbf{I}$, where ε is a small positive number, and $\mathbf{I}$ is an identity matrix. In (51), parameter λ is set to 1 for both stationary and Wiener PHN, since $\mathbf{R}$ and $\mathbf{p}$ are time-invariant for both cases.

In practice, $\theta[k]$ in (50) and (51) is unknown. Instead, $\hat{\theta}_e[k]$ in (31), the estimate of the PHN estimation error, is used to replace the actual error $\theta[k] - \hat{\theta}_{k|k-1}$ and drive the adaptive filter. Since $\mathrm{Im}[\xi_n](1 - \mathrm{Re}[\xi_n])$, the noise in $\hat{\theta}_e[k]$, is white and uncorrelated to the signal in Path II, the substitution of $\hat{\theta}_{k|k}$ for $\theta[k]$ does not affect the convergence to the optimum weights.

Figure 14 presents the convergence performance of the proposed adaptive scheme for stationary PHN. The signal pulse is root raised cosine with a roll-off factor of 0.3. The PHN bandwidth is set to 10 kHz and the PHN standard deviation is 5°. The initial filter weights for Path I and Path II are set to $1/N_1$ and 0, respectively. The values of all other parameters remain the same as those in Chapter 4. It is well known that the LMS algorithm is computationally simpler than the RLS algorithm, although longer time is required for LMS algorithm to converge. This is clearly observed in Figure 14. It takes about 400 iterations for the estimation error to converge using LMS algorithm; while it takes about 1000 iterations using RLS algorithm. It is noted that the convergence speed of the filter weights are different from that of the estimation error. Approximately 500 training symbols are required for the weights to converge in LMS algorithm while about 2000-3000 training

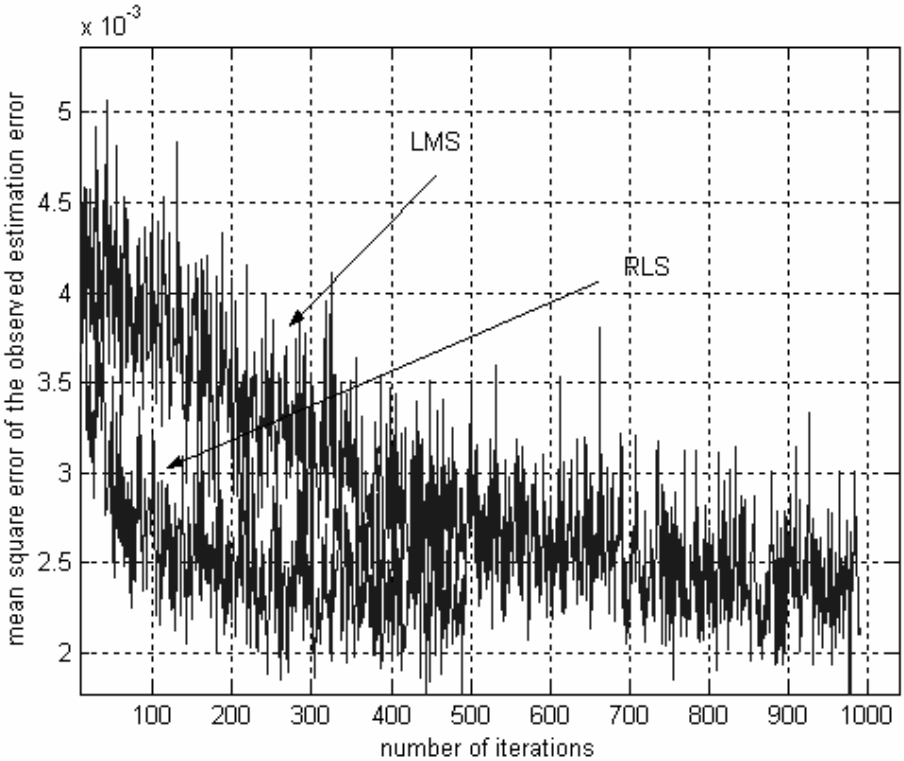

Figure 14. Simulation results on the convergence speed of estimation

symbols are required for the RLS algorithm, although the plots of the weights convergence are not shown.

Figure 15 presents the simulation results of the standard deviation of the noisy estimation error $\hat{\theta}_e[k]$ using the RLS and LMS algorithms and the corresponding theoretical values derived earlier. The PHN standard deviation changes from 0 to 15°. The performance is evaluated after convergence. Figure 15 shows a close match between simulation and analysis, and thus confirms the theoretical analysis in previous Chapter and the effectiveness of the employment of Path II. It can also be observed that the performance of the RLS and LMS algorithms are very close.

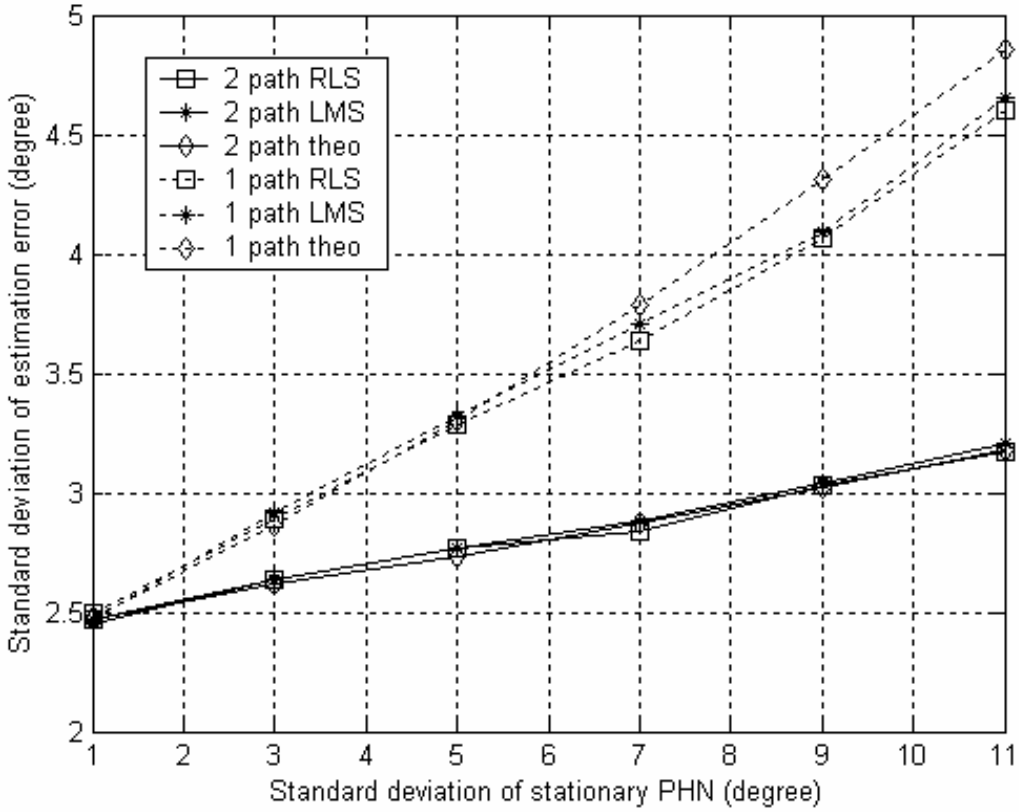

Figure 15. Simulation and theoretical results on standard deviation of estimation error $\hat{\theta}_e[k]$ for stationary PHN.

Therefore, only simulation results using RLS algorithm are shown subsequently, since those for LMS algorithm are similar. Although not shown, similar results are obtained for the Wiener PHN.

To further appreciate the significant improvement achieved by employing Path II, Figure 16 depicts the constellations of the received signal without PHN in Figure 16(a), the received signal contaminated by a stationary PHN of $\sigma_\phi = 5^o$ in Figure 16(b), the signal after RLS adaptive compensation using Path I only in Figure 16(c),

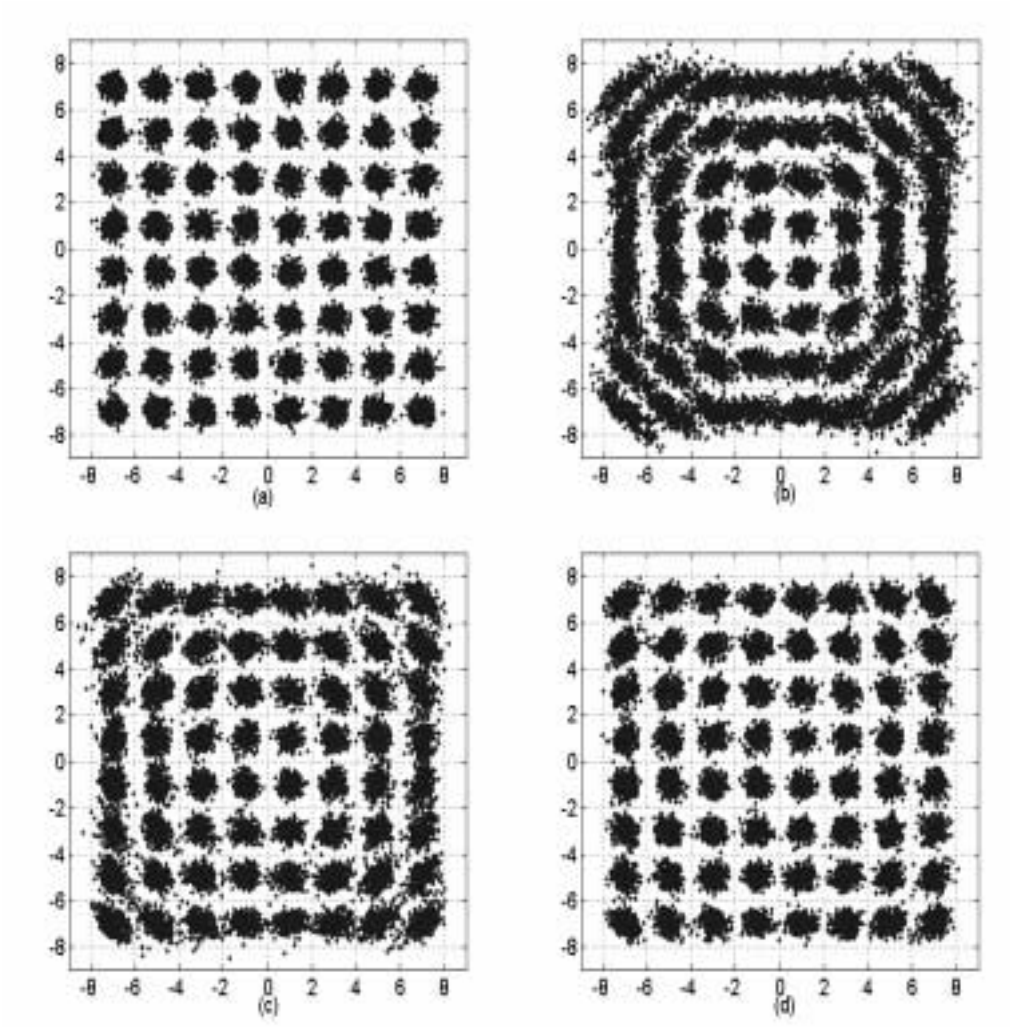

Figure 16. Constellation of the 64 QAM signal: (a) Without PHN (b) With stationary PHN, before compensation (c) After compensation using Path I (d) After compensation using both Path I and Path II

and the signal after RLS adaptive compensation using both Path I and Path II in Figure 16(d).

Figure 17 depicts the RLS simulation results on the symbol error rate (SER) vs. the input channel SNR_{in1} in Path I. Stationary PHN is applied with the standard

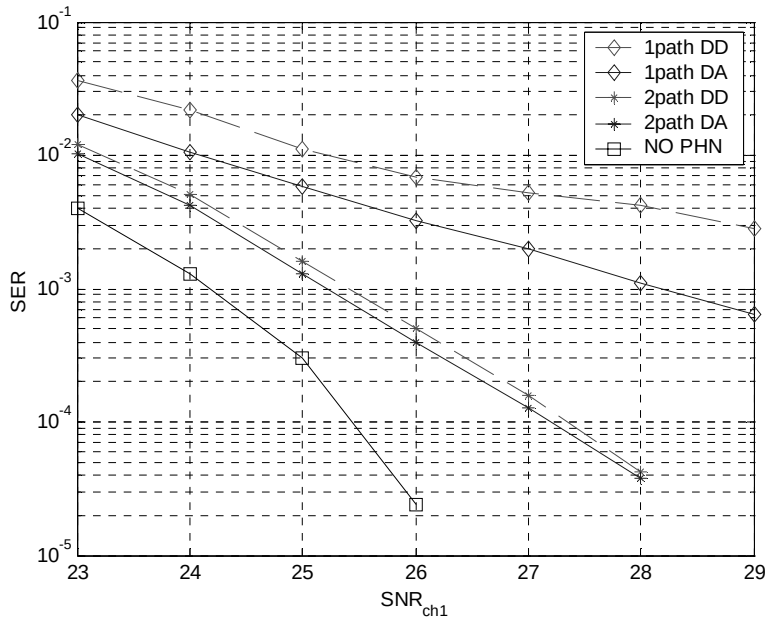

Figure 17. Simulation results on SER vs. SNR_{in1} for 64 QAM systems with stationary PHN.

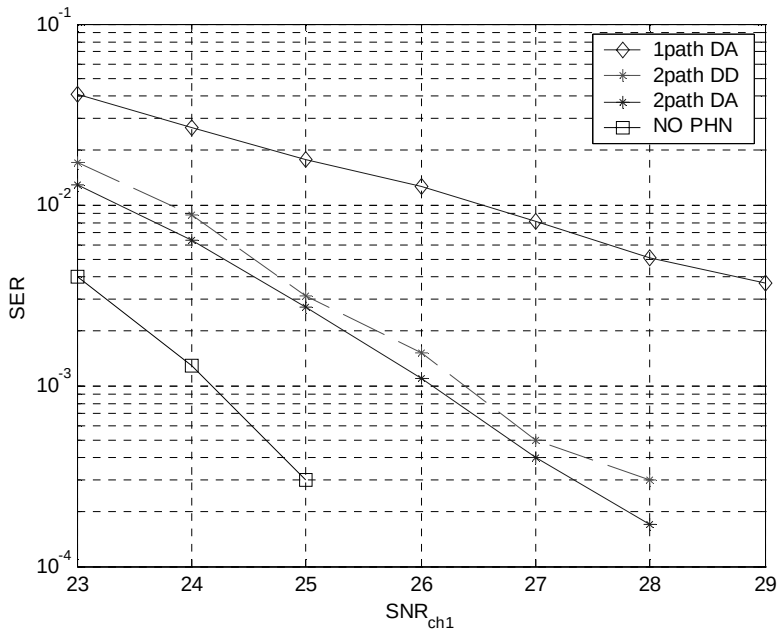

Figure 18. Simulation results on SER vs. SNR_{in1} of 64 QAM systems with Wiener PHN.

deviation and bandwidth being 5° and 5 kHz, respectively. The values of all other parameters remain the same as those set for Figure 15. The performance is evaluated after convergence. Both data-aided (DA, assuming all data are known and correct) and decision directed (DD, data are available from decision, and possibly include wrong decisions) [29] are simulated. DD mode is subject to decision error propagation and DA mode provides a lower bound for the performance. For 1-Path scheme, DD mode is at least 1 dB inferior to DA mode, while for 2-path scheme, performance of DD mode is close to that of DA mode. Performance of the 64 QAM system without PHN is also included. To reach SER=10^{-3}, the SNR_{in1} required for 2-Path scheme is only about 1dB higher than that required when there is no PHN, while the extra SNR_{in1} required for 1-Path scheme is about 4dB for DA mode (that for DD mode is even higher). For both 1-Path and 2-Path schemes, the extra SNR_{in1} becomes higher or lower when the PHN becomes heavier or lighter.

The performance in the presence of Wiener PHN is plotted in Figure 18, where the standard deviation per symbol $\sigma_\theta = 2^o$. Since the performance of the 1-Path scheme with DD mode is seriously degraded by error propagation, only DA mode is plotted for 1-Path case. Again, significant improvement of 2-Path scheme over 1-Path scheme can be observed.

5.2 Heterodyne Receivers and Lab Testing Results

Note that the proposed two-paths architecture, plotted in Figure 5(b) and re-drawn in Figure 19 (a) by taking out the conceptual delay in Path I, has an overhead of a delay element, a complex mixer, and an ADC. This structure is suitable for direct conversion receivers, also known as homodyne receivers, which have no intermediate frequency (IF) between the RF and the baseband. For heterodyne receivers where an IF is present in the receiver, the ADC can be replaced by an adder, as shown in Figure 19 (b). The carrier in Path I is $\omega_1 = \omega_0 + \omega_{IF1}$, where ω_{IF1} is the IF. In this architecture, Path I data is carried at the IF ω_{IF1} and the Path II data at the baseband in the analogue domain. The two paths can be separated in the digital domain by filtering and the rest of the signal processing remains unchanged. This structure can be simplified by removing the Path II mixer and adding the delayed and conjugated replica of the LO signal to the incoming signal before the Path I mixer, as shown in Figure 19 (c).

To further verify the proposed method against the real-life PHN data, a test bed using discrete components is established. A signal generator functions as the transmitter where data are generated, modulated, and then up-converted to the carrier frequency. A ring oscillator with heavy phase noise downconverts the signal to the IF. The down-converted and low-pass filtered data are then sampled by an oscillator and processed by MATLAB. Although the real-data version structure (slightly different from the complex data version shown before) depicted in Figure 20(a) is

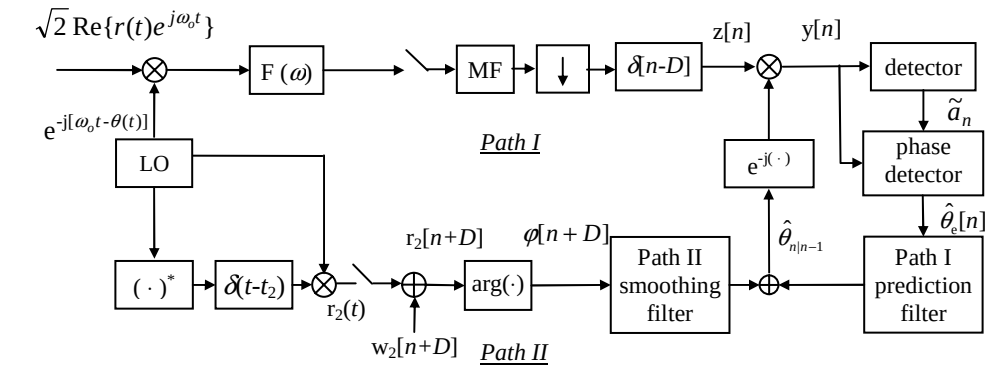

(a) Self-downconversion architecture for homodyne receivers

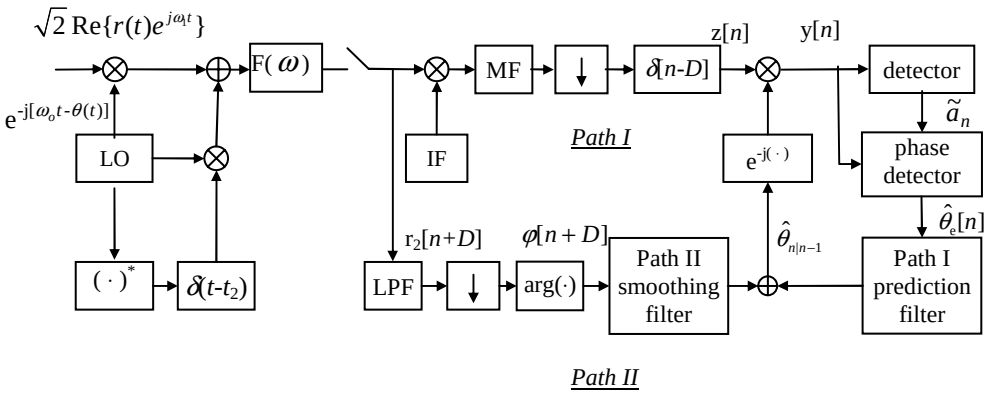

(b) Self-downconversion architecture for heterodyne receivers

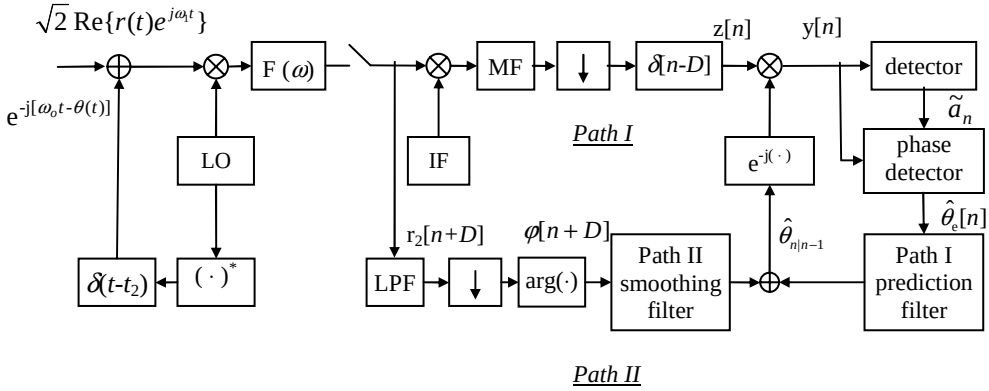

(c) Simplified structure for heterodyne receivers.

Figure 19. Heterodyne receivers with two paths.

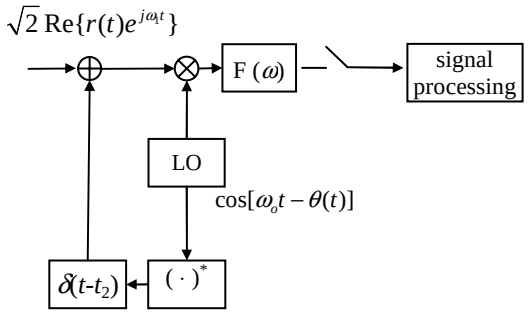

(a)

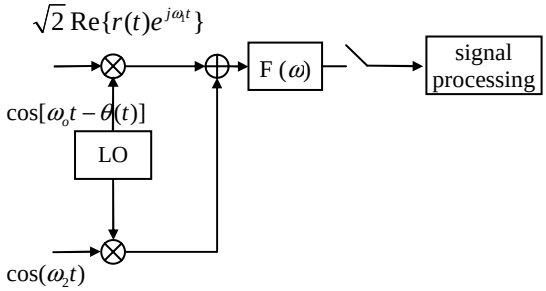

(b)

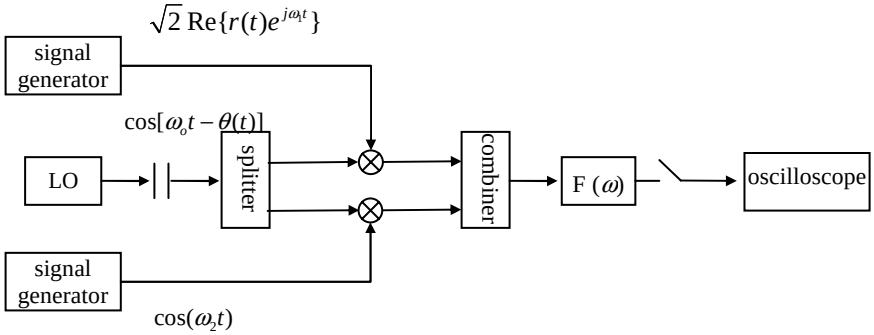

(c)

Figure 20 (a) Block diagram (real-valued version). (b) Block diagram for the test bed. (c) Component level schematic for the test bed

close to the proposed structure, it has some difficulties with the equipments available and the discrete components: 1) the baseband PHN signal is hard to be sampled by the oscilloscope due to the ambient noise; 2) It does not have the flexibility to change the delay in the self-downconversion structure.

Since the main purpose of this experiment is to test the proposed method on real PHN data, a simplified structure is employed, with the block diagram and the component level schematic shown in Figure 20 (b) and Figure 20 (c), respectively. In this setup, a second signal generator is used to bring the LO output to another IF ω_{IF2}. Since the PHN of the signal generator is much weaker than the LO, the combined Path II PHN comes mainly from the LO. The complete PHN instead of the difference of the PHN is sampled and available. The self-downconversion is performed in MATLAB, thus provides more flexibility in changing the delay and the goal of obtaining real-life PHN data is easily met.

Another difference from the previous simulations is the modulation scheme. In the lab experiment, BPSK is employed instead of 64QAM in that it is easier to process and can equivalently demonstrate the effect of PHN compensation. The blocking capacitor added in Figure 20 (c) is to filter out the DC component from the actual LO output.

Since the ring oscillator employed in the test is a free-running oscillator, the frequency keeps changing over time. The PHN here is the Wiener PHN with the symbol increment $\sigma_\theta = 4^o$. The frequency of the LO is around 1.5 GHz. The IF for Path I is 50 MHz. The IF for Path II is 75 MHz. The LPF has a 3 dB bandwidth at

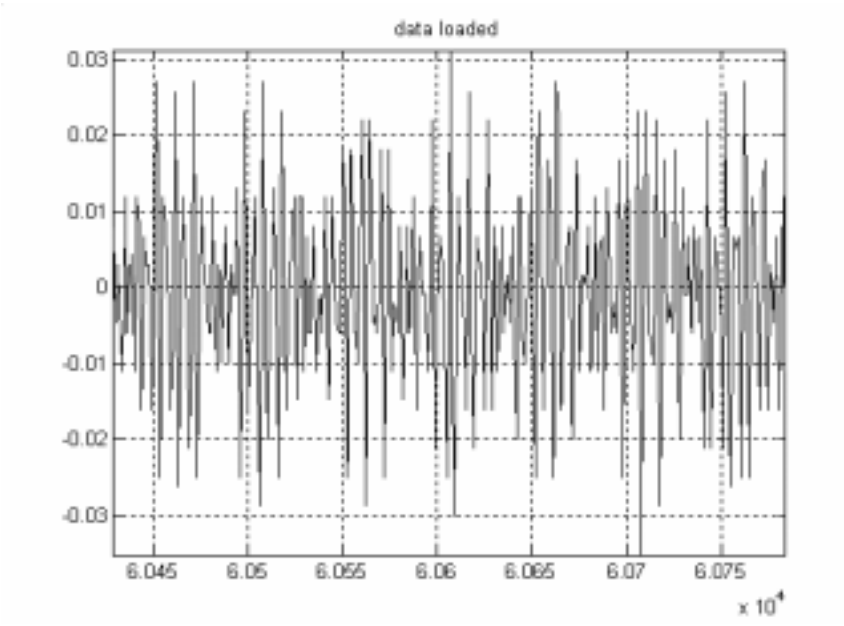

Figure 21. Sampled data in time domain

100 MHz. The sampling frequency at the oscilloscope is 250 MHz. Approximately 100k data can be sampled by the oscilloscope each time. The BPSK data has a symbol rate of 5 MHz. The root raised cosine pulse shaping filter has a roll-off factor of 0.3. Figure 21 shows a segment of the sampled data at the LPF output.

Without PHN tracking, the constellation is a circle due to the Wiener PHN as shown in Figure 22(a). The recovered constellation using the proposed two-paths method and the conventional one-path method are show in Figure 22(b)(c). The SNR after compensation for the proposed method and the conventional method is 25.9 dB and 22.9 dB, respectively, which is a 3 dB improvement. For comparison purpose, a second order digital PLL (DPLL) is also tried and results in an SNR of 22.7 dB as shown in Figure 22 (d). The proposed method demonstrates significant improvement over conventional PHN compensation and phase tracking schemes.

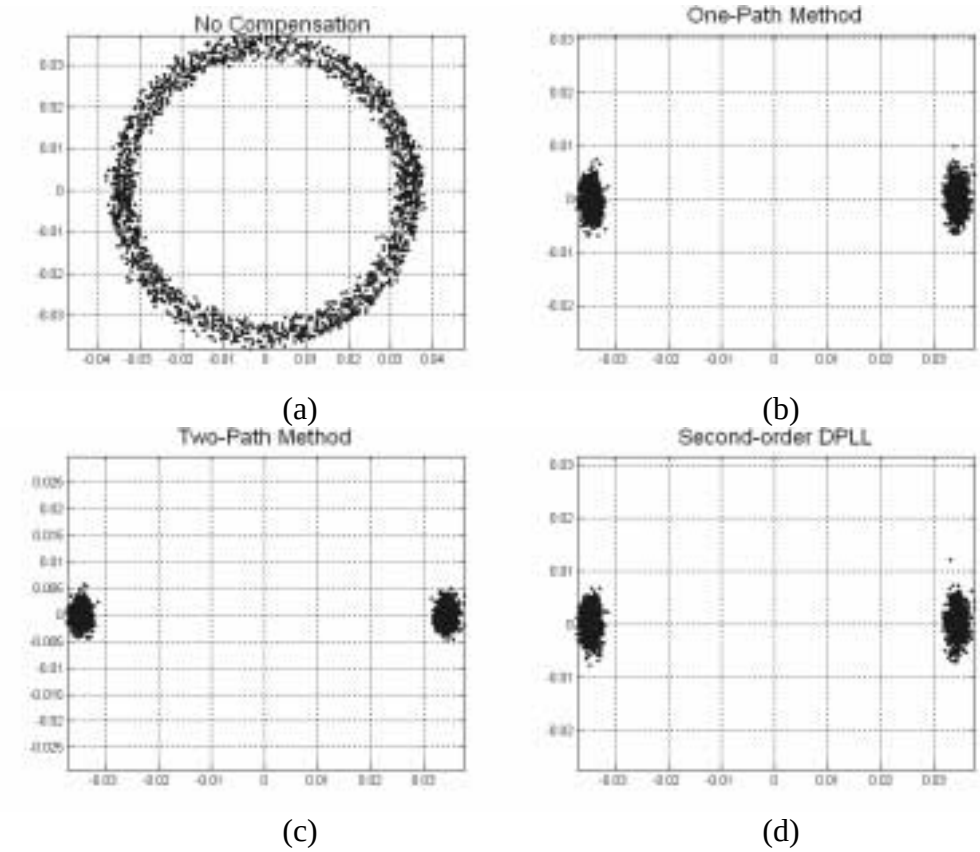

Figure 22. Constellation for Lab test BPSK signal:

(a) Without PHN compensation. (b) After compensation using Path I.

(c) After compensation using both Path I and Path II.

(d) After compensation using DPLL

Chapter 6

Transmitter Phase Noise Compensation

6.1 Self-downconversion structure for transmitter

The idea of self-downconversion can be applied to compensate the transmitter PHN as well. Figure 23 shows an overview of a general digital communication transmitter equipped with the proposed PHN compensation scheme. The mapped data a_n with symbol period T is fed into the digital pulse shaping filter (DPSF). The DPSF first upsamples the data to the sampling rate $1/T_s$ and then passes them through a pulse shaping filtering. The DPSF output is denoted as b_m. Recall that index n is used to represent the discrete-time index at the symbol rate, while index m is used for those at the sampling rate. PHN compensation follows the DPSF:

$$p_m = b_m e^{-j\hat{\theta}[m]} \tag{52}$$

where p_m denotes the compensated sample and $\hat{\theta}[m]$ is the PHN estimate. After D/A conversion, the continuous-time signal $p(t)$ is upconverted to the carrier frequency:

$$s(t) = p(t)e^{j(\omega_o t + \theta(t))}. \tag{53}$$

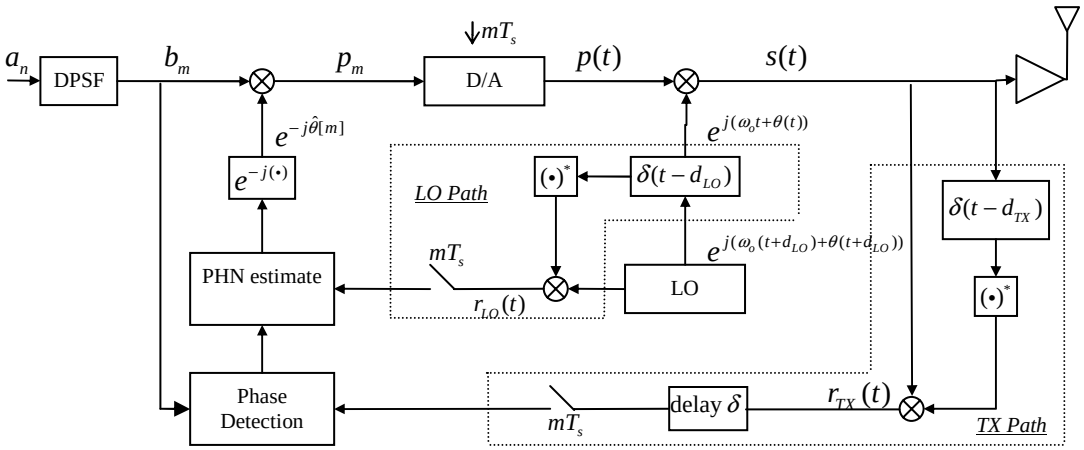

Figure 23. The self-downconversion transmitter architecture.

Notice that in (53), the LO output has the PHN . As a result of PHN compensation, transmitted signal exhibits some remaining PHN as a result of the PHN estimation error. At the transmitter, the goal of PHN compensation is not to minimize the estimation error, but to keep it constant, since the constant phase difference can be removed at the receiver during phase recovery.

In the proposed PHN compensation scheme, two additional paths are added for PHN estimation as shown in Figure 23. They are called LO Path and TX Path, respectively. They downconvert the signals at passband to baseband by self-downconversion, i.e., mixing themselves with a delayed and conjugated replica. The corresponding hardware overhead should be modest, especially in integrated circuits. Although the passband signal or the LO signal can be directly sampled at a fraction of the carrier frequency, such subsampling scheme would be overly sensitive to sampling jitter because of the high carrier frequency.

The motivation for adding the LO path is to have access to future PHN information. Ideally, if the delay added by the delay element in the LO Path $d_{LO} = T_s$, the LO Path can provide perfect PHN estimate by adding the new PHN difference from LO Path to the previous estimate. However, such an accurate delay block is difficult to implement and therefore not practical. The TX Path is added to provide an error signal that can be used to adapt the estimation filter. In summary, the LO Path, which provides future PHN information, serves as the input of the PHN estimation filter, while the TX Path provides the estimation error information to adaptively update the estimation filter.

6.2 Transmitter PHN Estimation: LO Path

When modulating the signal $p(t)$, the delayed version of the LO signal is used. This enables access to future PHN information, which can be used to improve the PHN estimation. The output of the self-downconversion mixer in the LO Path is

$$r_{LO}(t) = e^{j(\theta(t+d_{LO})-\theta(t)+\omega_o d_{LO})} \triangleq e^{j(\theta(t+d_{LO})-\theta(t)+\gamma_{LO})}, \tag{54}$$

where d_{LO} is the delay added by the delay element as shown in Figure 23, and the constant $\omega_o d_{LO}$ is denoted by γ_{LO}. Although the exact d_{LO} is unknown, we assume that it is designed to be larger than T_s. Sampling the LO Path output at $1/T_s$:

$$r_{LO}[m] = r_{LO}(mT_s) = e^{j(\theta(mT_s+d_{LO})-\theta(mT_s)+\gamma_{LO})}. \tag{55}$$

The phase of $r_{LO}[m]$,

$$\varphi_{LO}[m] = \arg(r_{LO}[m]) = \theta(mT_s + d_{LO}) - \theta(mT_s) + \gamma_{LO}, \tag{56}$$

provides the input of the PHN estimation filter, where arg(·) stands for "the argument of". Note that $\varphi_{LO}[m]$ has future PHN information $\theta(mT_s + d_{LO})$, which can be used to improve the estimation of the PHN. The phase difference in (56) is stationary, regardless of whether PHN is a stationary or a Wiener process. To improve the estimation accuracy, the constant γ_{LO} in (56), which can be obtained (e.g. by a moving average filter), is subtracted from $\varphi_{LO}[m]$. In case γ_{LO} is close to π and $\varphi_{LO}[m]$ appears to be around π or $-\pi$, $r_{LO}[m]$ can be pre-multiplied by -1 and then the $\arg(\bullet)$ can be applied without the π boundary problems. Therefore, we obtain (γ_{LO} is subsequently ignored):

$$\varphi_{LO}[m] = \arg(r_{LO}[m]) = \theta(mT_s + d_{LO}) - \theta(mT_s)\,. \tag{57}$$

6.3 Transmitter PHN Estimation: TX Path

Similar to what happens in the LO Path, the transmitted signal is downconverted to the baseband in the TX Path. The resulting output is

$$\begin{aligned} r_{TX}(t) &= s(t-\delta)s^*(t-\delta-d_{TX}) \\ &= p(t-\delta)\,p^*(t-\delta-d_{TX})e^{j(\theta(t-\delta)-\theta(t-\delta-d_{TX})+\gamma_{TX})}, \end{aligned} \tag{58}$$

where δ is the delay introduced by the circuits (see Figure 23), d_{TX} is the delay added by the self-downconversion in the TX Path, and $\gamma_{TX} \triangleq \omega_o d_{TX}$. Sampling $r_{TX}(t)$ at rate $1/T_s$ yields:

$$\begin{aligned} r_{TX}[m] &= r_{TX}(mT_s) \\ &= p(mT_s-\delta)\,p^*(mT_s-\delta-d_{TX})e^{j(\theta(mT_s-\delta)-\theta(mT_s-\delta-d_{TX})+\gamma_{TX})}. \end{aligned} \tag{59}$$

Assuming $\delta < T_s$, $p(mT_s - \delta)$ and $p(mT_s - \delta - d_{TX})$ in (59) can be linearly approximated as

$$p(mT_s - \delta) \approx (x_1 b_m + y_1 b_{m-1}) e^{-j(x_1 \hat{\theta}[m] + y_1 \hat{\theta}[m-1])} \tag{60}$$

$$p(mT_s - \delta - d_{TX}) \approx (x_2 b_{m-d_1} + y_2 b_{m-d_2}) e^{-j(x_2 \hat{\theta}[m-d_1] + y_2 \hat{\theta}[m-d_2])} \tag{61}$$

where $d_1 = \lfloor \delta + d_{TX} \rfloor$, $d_2 = d_1 + 1$, $y_1 = \delta / T_s$, $x_1 = 1 - y_1$, $y_2 = (\delta + d_{TX} - d_1)/T_s$, $x_2 = 1 - y_2$ and $\lfloor \bullet \rfloor$ stands for "the integer part of". Applying (60) and (61) into (59), the signal in TX Path becomes

$$\begin{aligned} r_{TX}[m] \approx\ & (x_1 b_m + y_1 b_{m-1})(x_2 b^*_{m-d_1} + y_2 b^*_{m-d_2}) \cdot \\ & e^{j(\theta(mT_s - \delta) - x_1 \hat{\theta}[m] - y_1 \hat{\theta}[m-1] - \theta(mT_s - \delta - d_{TX}) + x_2 \hat{\theta}[m-d_1] + y_2 \hat{\theta}[m-d_2] + \gamma_{TX})}. \end{aligned} \tag{62}$$

Since the data b_m are available at the transmitter, the phase term in (62) can be obtained by

$$\begin{aligned} \varphi_{TX}[m] &= \arg((x_1 b^*_m + y_1 b^*_{m-1})(x_2 b_{m-d_1} + y_2 b_{m-d_2}) r_{TX}[m]) \\ &\approx \theta(mT_s - \delta) - x_1 \hat{\theta}[m] - y_1 \hat{\theta}[m-1] - \theta(mT_s - \delta - d_{TX}) + x_2 \hat{\theta}[m-d_1] + y_2 \hat{\theta}[m-d_2]. \end{aligned} \tag{63}$$

The constant γ_{TX} is ignored in (63) since it can be removed, similar to γ_{LO}. The quantities x_1 and x_2 in (63), and therefore y_1 and y_2, can be readily obtained by maximizing the correlation between $(x_1 b^*_m + y_1 b^*_{m-1})(x_2 b_{m-d_1} + y_2 b_{m-d_2})$ and $r_{TX}[m]$. Note that $(x_1 b^*_m + y_1 b^*_{m-1})(x_2 b_{m-d_1} + y_2 b_{m-d_2})$ needs to be normalized before correlation.

Let $\theta_e(t)$ be the continuous time PHN estimation error with

$$\theta_e(mT_s) = \theta_e[m] = \theta(mT_s) - \hat{\theta}[m]. \tag{64}$$

Then (63) can be approximately expressed as

$$\varphi_{TX}[m] \approx \theta_e(mT_s - \delta) - \theta_e(mT_s - \delta - d_{TX}). \tag{65}$$

From (65), $\varphi_{TX}[m]$ is the difference of the PHN estimation error at two different time instances. Recall that the objective of transmitter PHN compensation is to keep $\theta_e(t)$ constant. However, since $\theta_e(t)$ is not directly accessible, $\varphi_{TX}[m]$ is used instead to provide an error signal to adapt the PHN estimation.

Define

$$\Delta[m] \triangleq \theta(mT_s - \delta) - \theta(mT_s - \delta - d_{TX}) \tag{66}$$

as the change in PHN from time $mT_s - d_{TX}$ to mT_s. Similar to $\varphi_{LO}[m]$ in (56), $\Delta[m]$ is stationary for both stationary and Wiener PHN. Equation (63) now becomes

$$\varphi_{TX}[m] = \Delta[m] - x_1\hat{\theta}[m] - y_1\hat{\theta}[m-1] + x_2\hat{\theta}[m-d_1] + y_2\hat{\theta}[m-d_2]. \tag{67}$$

6.4 Transmitter PHN Estimation

Suppose we want to estimate $\hat{\theta}[m+1]$ with information up to time m, (67) provides a guideline to minimize $\varphi_{TX}[m]$:

$$\hat{\theta}[m+1] = (\Delta[m+1] - y_1\hat{\theta}[m] + x_2\hat{\theta}[m-d_1+1] + y_2\hat{\theta}[m-d_2+1])/x_1 \tag{68}$$

Note that at time m, only $\Delta[\mathrm{m+1}]$ is unavailable on the right side of (68). However, $\Delta[\mathrm{m+1}]$ can be estimated from $\varphi_{LO}[m-i]$, $i \geq 0$, which is available at this time. The relationship between $\varphi_{LO}[m]$, $\varphi_{TX}[m]$, $\Delta[\mathrm{m}]$ and $\theta[m]$ is illustrated in Figure 24. The value of $\Delta[\mathrm{m+1}]$ can be estimated from the observation:

$$\mathbf{\theta}_m = [\varphi_{LO}[m] \quad \varphi_{LO}[m-1] \quad \cdots \quad \varphi_{LO}[m-N+1]]^T \tag{69}$$

by a finite-response-filter (FIR) filter:

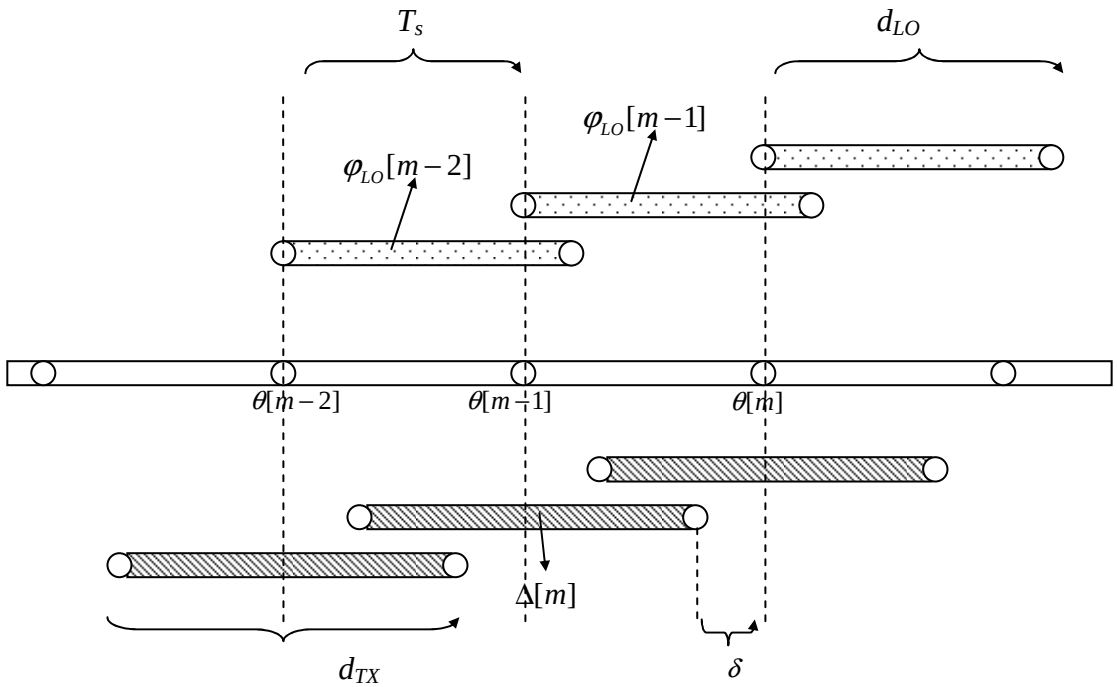

Figure 24. Relationship of $\varphi_{LO}[m-1]$ and $\Delta_\theta(m, d_{TX})$ in time.

$$\hat{\Delta}[\mathrm{m}] = \mathbf{w}^T \boldsymbol{\theta}_m, \tag{70}$$

where N is the length of the estimation filter and $\mathbf{w}$ is the vector of the filter weights. Since both $\Delta[\mathrm{m+1}]$ and $\boldsymbol{\theta}_m$ are stationary, the optimal weight vector $\mathbf{w}_o$ can be decided by Wiener filtering:

$$\mathbf{w}_o = (E[\boldsymbol{\theta}_m \boldsymbol{\theta}_m^T])^{-1} E[\Delta[\mathrm{m+1}]\boldsymbol{\theta}_m]. \tag{71}$$

Therefore, $\hat{\theta}[m+1]$ can be obtained by

$$\begin{aligned}\hat{\theta}[m+1] &= (\hat{\Delta}[\mathrm{m+1}] - y_1\hat{\theta}[m] + x_2\hat{\theta}[m-d_1+1] + y_2\hat{\theta}[m-d_2+1])/x_1 \\ &= (\mathbf{w}^T\boldsymbol{\theta}_m - y_1\hat{\theta}[m] + x_2\hat{\theta}[m-d_1+1] + y_2\hat{\theta}[m-d_2+1])/x_1.\end{aligned} \tag{72}$$

The Wiener filtering in (71) requires a priori statistical information that is often not available or keeps changing during the PHN estimation operation. The TX Path

signal $\varphi_{TX}[m]$ provides an estimation error and makes adaptive adjustment of the weights possible, which can be seen by substituting the estimate $\hat{\theta}[m]$ according to (72) into (67):

$$\varphi_{TX}[m] = \Delta[\mathrm{m}] - \hat{\Delta}[\mathrm{m}]. \tag{73}$$

It is clear that the output $\varphi_{TX}[m]$ from the TX Path provides the estimation error of $\hat{\Delta}[\mathrm{m}]$. With the future PHN information provided in the LO Path and the estimation error supplied by the TX Path, various adaptive algorithms can be devised [20]. In this work, only the well-known least-mean-square (LMS) is shown for its simplicity. The LMS PHN estimation procedure is:

$$\varphi_{TX}[m] = \arg\left((x_1 b_m^* + y_1 b_{m-1}^*)(x_2 b_{m-d_1} + y_2 b_{m-d_2}) r_{TX}[m]\right) \tag{74}$$

$$\mathbf{w}_m = \mathbf{w}_{m-1} + \mu \varphi_{TX}[m] \boldsymbol{\theta}_{m-1} \tag{75}$$

$$\hat{\theta}[m+1] = (\mathbf{w}_m^T \boldsymbol{\theta}_m - y_1 \hat{\theta}[m] + x_2 \hat{\theta}[m-d_1+1] + y_2 \hat{\theta}[m-d_2+1])/x_1 \tag{76}$$

where μ is the step size.

It is important to mention that the proposed PHN compensation scheme works for both Wiener PHN and stationary PHN, as the type of the PHN is not assumed in the derivation of the PHN estimation.

Chapter 7

Performance of Transmitter PHN Compensation

7.1 Simulation Results

To illustrate the effectiveness of the proposed transmitter PHN compensation scheme, numerical simulation results of PHN estimation are presented. The symbol period T is assumed to be 10^{-6} s and the sampling period $T_s = T/4$. Without loss of generality, the delays of LO Path and TX Path are set to be equal $d_{LO} = d_{TX} = 1.2T_s$ and δ is set to zero for simplicity. Although the proposed method works effectively for both Wiener PHN and stationary PHN, only results for Wiener PHN are presented. The σ_θ for the PHN is 1°. There are 4 taps in the PHN estimation filter. The initial weights for the LMS filter are set to be [0.5 0.5 0 0]. The step size is 25 in the initial stage and 10 thereafter. A total of 20000 symbols are simulated.

Figure 25 depicts the time domain PHN at the sampling rate and the PHN estimate. The remaining PHN (estimation error) is also shown in Figure 25. It can be observed that the PHN is greatly reduced. The improvement is further demonstrated in the frequency domain as shown in Figure 26, where the PSD of the PHN before and after compensation is plotted. It can be observed that the proposed PHN compensation scheme results in an improvement of about 8-10 dB in the PSD. Figure 27 depicts the weights adaptation of the LMS filter. It took about 1500 samples for the

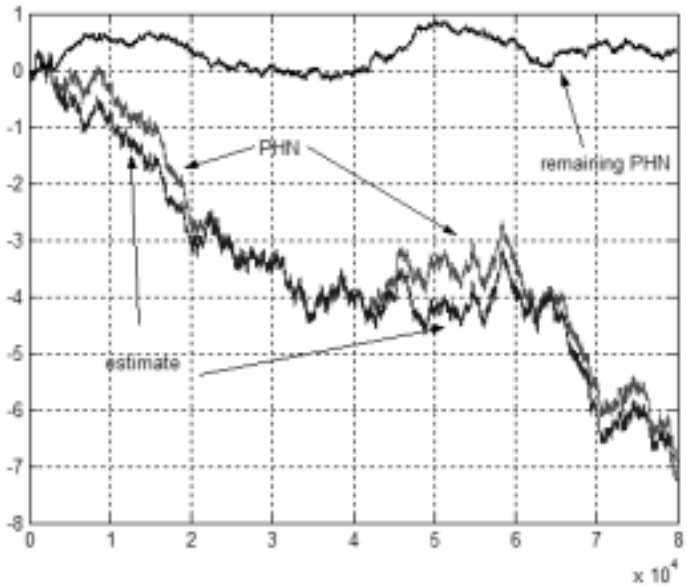

Figure 25. Time domain Wiener PHN: The PHN, the PHN estimate, and the remaining PHN.

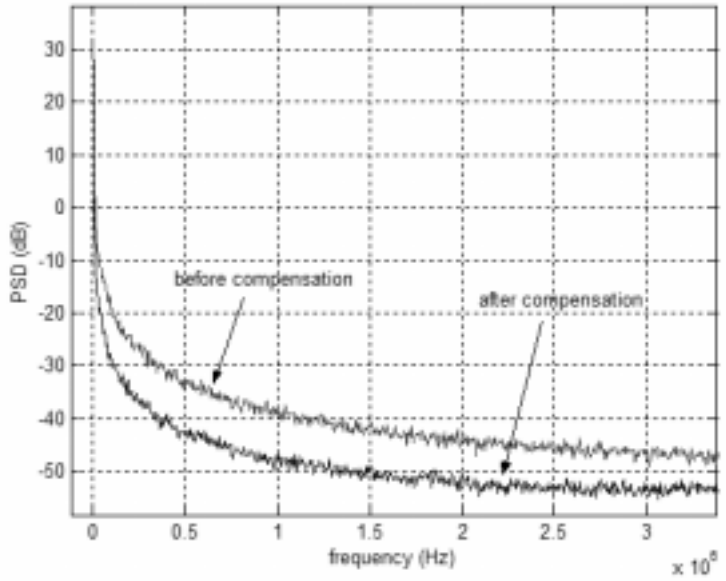

Figure 26. Power Spectrum Density of Wiener PHN: Before and after compensation

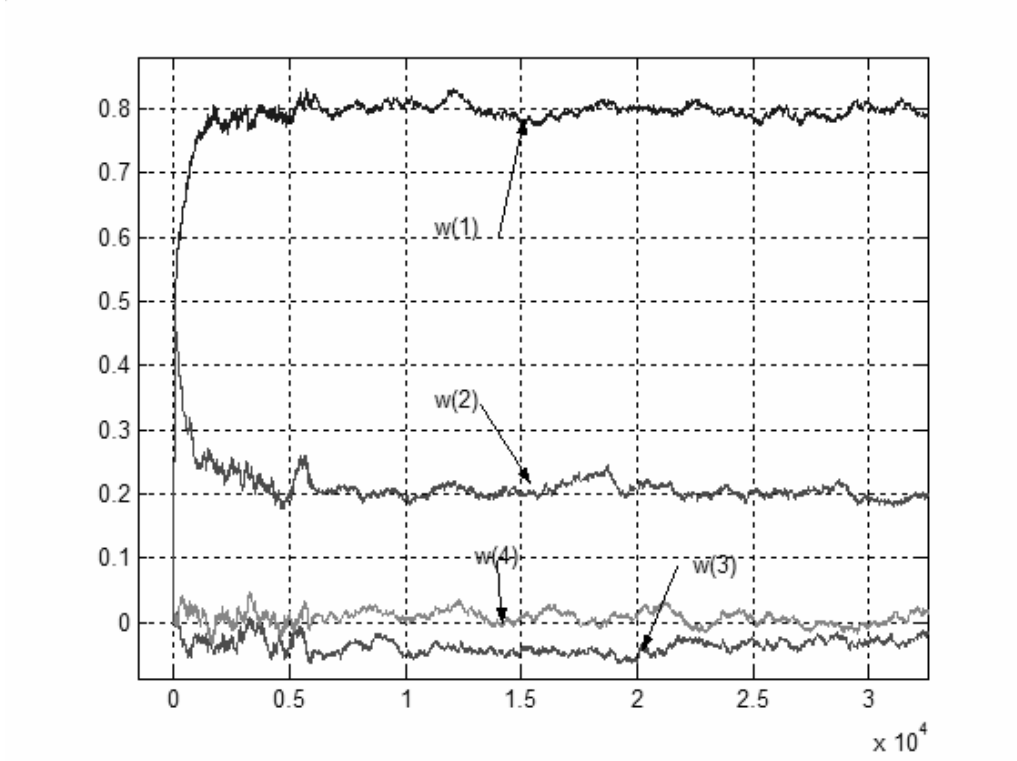

Figure 27. Tap weights of the LMS PHN estimation filter.

weights to converge. Although not shown, similar plots can be obtained for the stationary PHN.

7.2 Estimation Error Analysis

The error $\varphi_{TX}[m]$ in estimating $\Delta[m]$ is minimized in the MMSE sense. It is Gaussian with zero mean and variance

$$Var[\varphi_{TX}[m]] = Var[\Delta[m]] - E[\Delta[m]\boldsymbol{\theta}_{m-1}^{T}]\mathbf{w}_o \tag{77}$$

The spectrum of $\varphi_{TX}[m]$ is derived in Section 7.3. Note that in this section, the physical delay from circuits δ, which is small compared to T_s, is assumed to be zero

for simplicity and its effects can be readily added to the analysis presented. Consequently, x_1 and y_1 becomes 1 and 0 respectively.

The filter described in (70) and (71) estimates $\Delta[m]$, which is an intermediate step to obtain the desired PHN estimate $\hat{\theta}[m]$ as is shown in (72). Therefore, it is the estimation error $\theta_e[m]$ in estimating $\theta[m]$ that is affecting the transmitted signal. From (64) and (72), $\theta_e[m]$ can be expressed as

$$\begin{aligned}\theta_e[m] &= \theta(mT_s) - (\hat{\Delta}_\theta(m, d_{TX}) + x_2\hat{\theta}[m-d_1] + y_2\hat{\theta}[m-d_2]) \\ &= \theta(mT_s) - \Delta_\theta(m, d_{TX}) + \varphi_{TX}[m] - x_2\hat{\theta}[m-d_1] - y_2\hat{\theta}[m-d_2] \\ &= \theta(mT_s - d_{TX}) - x_2\hat{\theta}[m-d_1] - y_2\hat{\theta}[m-d_2] + \varphi_{TX}[m] \\ &\approx x_2\theta_e[m-d_1] + y_2\theta_e[m-d_2] + \varphi_{TX}[m]\end{aligned} \tag{78}$$

The last line of (78) is obtained by approximating $\theta(mT_s - d_{TX})$ by

$$\theta(mT_s - d_{TX}) \approx x_2\theta[m-d_1] + y_2\theta[m-d_2]. \tag{79}$$

From (78), it is clear that $\theta_e[m]$ is an auto-regression (AR) process with $\varphi_{TX}[m]$ as the input. The PHN estimation error $\theta_e[m]$ is a zero-mean Gaussian process. Since $x_2 + y_2 = 1$, the system function for (78)

$$H(z) = \frac{1}{1 - x_2 z^{-d_1} - y_2 z^{-d_2}} \tag{80}$$

has a root at $z = 1$ Therefore, the residue PHN $\theta_e[m]$ is non-stationary. This nonstationarity is reflected at the infinite frequency response at frequency $f = 0$. Similar to the case in Wiener PHN, the phasor $e^{j\theta_e[m]}$ can be approximately assumed stationary. Although the rigid method to calculate PSD of $e^{j\theta_e[m]}$ is possible, similar to that of Wiener PHN, it is much more complicated and a simple heuristic method is

employed to understand the factors that affect the residue PHN. Although $\theta_e[m]$ is non-stationary, its PSD is very close to the PSD of $e^{j\theta_e[m]}$ except at $f=0$ because the value of $\theta_e[m]$ is small. The spectrum of $\theta_e[m]$, ignoring the zero frequency, would be decided both by the spectrum of $\varphi_{TX}[m]$ and by the frequency response of $H(z)$. The former is derived in Section 7.3, and the latter is approximately decided by the delay in TX Path d_{TX}, which manifests itself as x_2, y_2, d_1 and d_2 (80). In such cases, the spectrum will have small sidelobes due to the frequency response of (80). Figure 28 and Figure 29 demonstrate the role of d_{TX} in determine the shape of the residue PHN spectrum. Attention should be paid in determining d_{TX} to avoid sidelobes.

7.3 The spectrum of $\varphi[m]$

The spectrum of the estimation error in (70) and (73) is derived in this section. From (73), $\varphi_{TX}[m]$, the error in estimating $\Delta[m]$ and its autocorrelation are

$$\varphi_{TX}[m] = \Delta[m] - \sum_{i=1}^{d_2} w_i \varphi_{LO}(m-i) \tag{81}$$

$$\begin{aligned}
R_\varphi[l] &\triangleq E[\varphi_{TX}[m]\varphi_{TX}[m-l]] \\
&= E[[\Delta[m] - \sum_{i=1}^{d_2} w_i \varphi_{LO}(m-i)][\Delta[m-l] - \sum_{i=1}^{d_2} w_i \varphi_{LO}(m-l-i)]] \\
&= E[\Delta[m]\Delta[m-l]] + E[\sum_{i=1}^{d_2} w_i \varphi_{LO}(m-i) \sum_{i=1}^{d_2} w_i \varphi_{LO}(m-l-i)] \\
&\quad - \sum_{i=1}^{d_2} w_i E[\Delta[m-l]\varphi_{LO}(m-i)]] - \sum_{i=1}^{d_2} w_i E[\Delta[m]\varphi_{LO}(m-l-i)] \\
&\triangleq R_\Delta[l] + R_w[l] - R_1[l] - R_2[l]
\end{aligned} \tag{82}$$

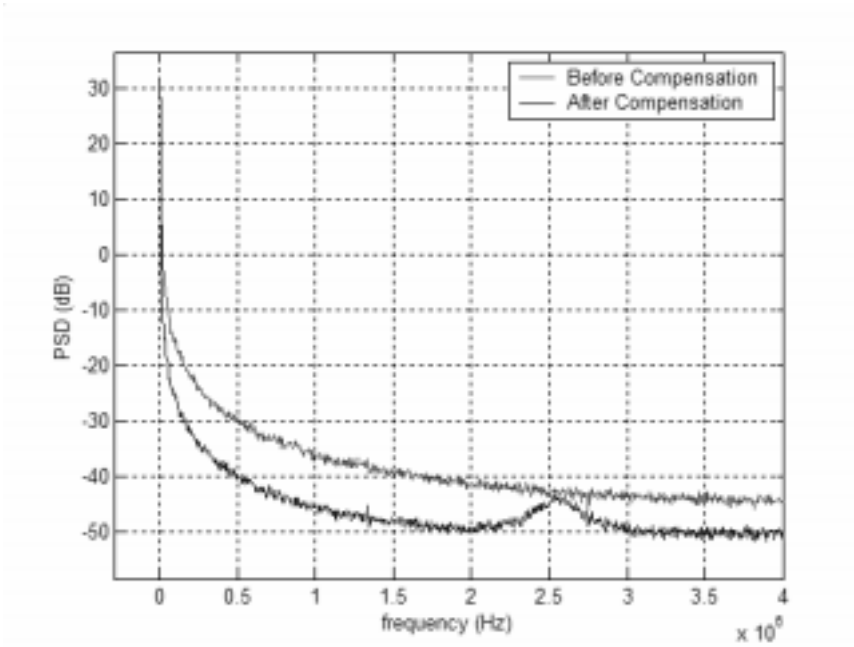

(a)

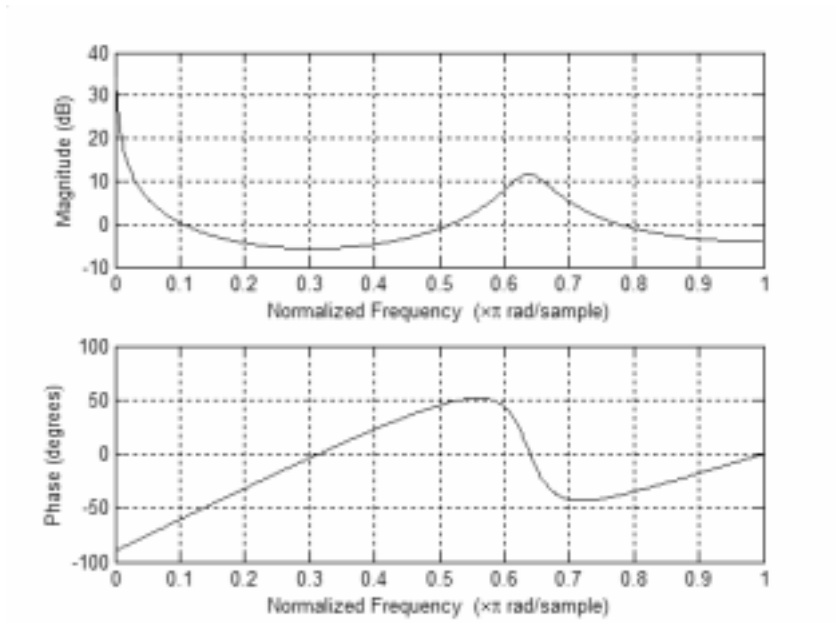

Figure 28. (a) Spectrum of remaining PHN when $d_{TX} = 3.2T_s$ and $d_{LO} = 1.2T_s$

(b) the corresponding frequency response of filter in (80)

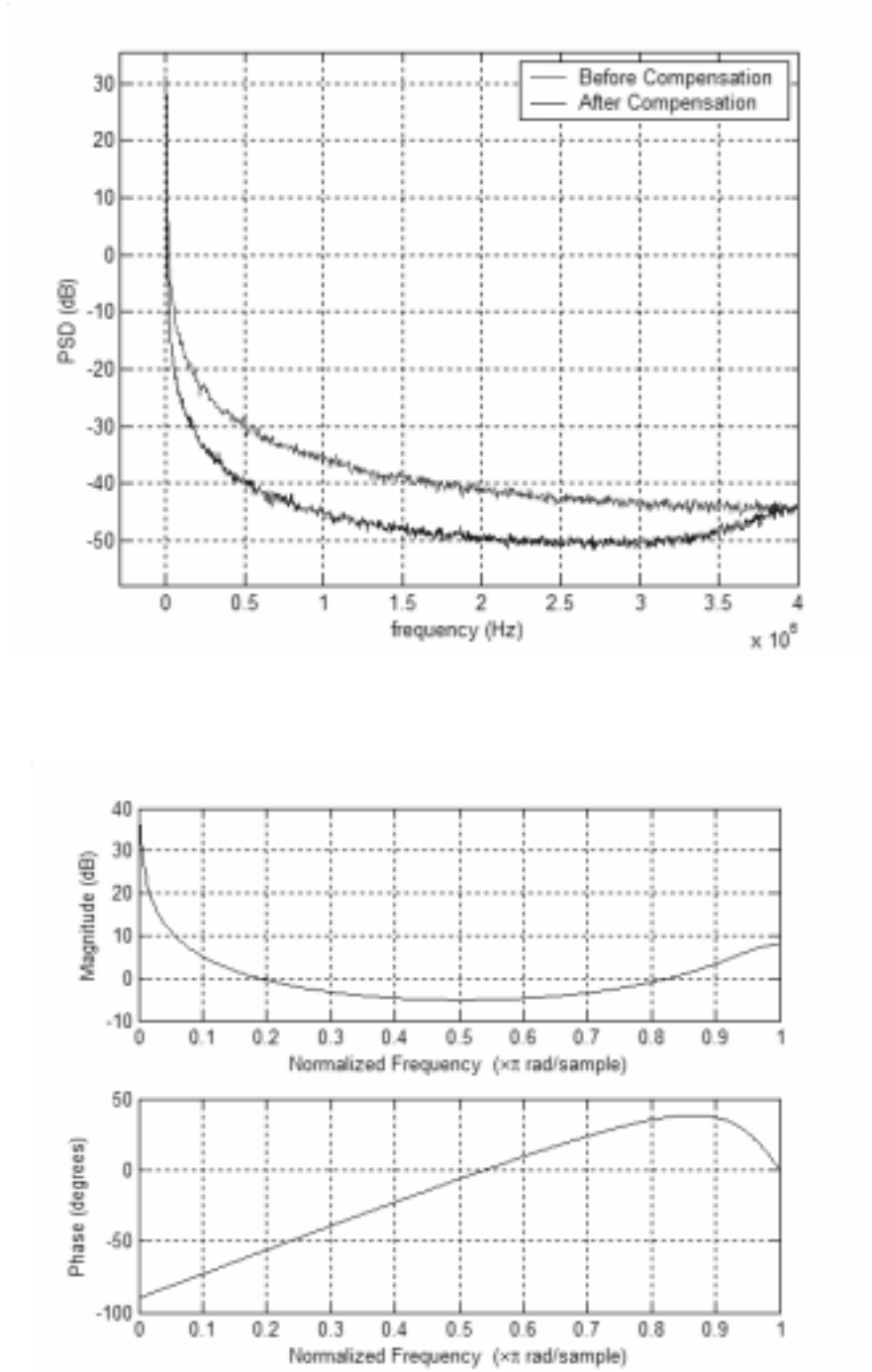

Figure 29. (a) Spectrum of remaining PHN when $d_{TX} = 1.8T_s$ and $d_{LO} = 1.2T_s$

(b) the corresponding frequency response of filter in (80)

For Wiener PHN, $R_{\Delta}[l]$, the first term in (82), can be readily obtained by referring to Figure 24

$$R_{\Delta}[m] = \begin{cases} \sigma_{\theta}^{2} \dfrac{d_{TX} - |m| T_s}{T}, & -l_{TX} \le m \le l_{TX} \\ 0, & otherwise \end{cases} \tag{83}$$

where $l_{TX} \triangleq \lfloor d_{TX} / T_s \rfloor$. By defining the auto-correlation of the estimation filter input $\varphi_{LO}[m]$:

$$R_{LO}[l] \triangleq E[\varphi_{LO}[m]\varphi_{LO}[m-l]], \tag{84}$$

the second term in (82) can be obtained by

$$R_{w}[l] = R_{LO}[l] * w[l] * w[-l], \tag{85}$$

where

$$w[l] = \begin{cases} w_l, & 1 \le m \le d_2 \\ 0, & otherwise \end{cases} \tag{86}$$

are the extended filter weights. Similar to $R_{\Delta}[l]$, $R_{LO}[l]$ also has a triangular shape:

$$R_{LO}[m] = \begin{cases} \sigma_{\theta}^{2} \dfrac{d_{LO} - |m| T_s}{T}, & -l_{LO} \le m \le l_{LO} \\ 0, & otherwise \end{cases} \tag{87}$$

where $l_{LO} \triangleq \lfloor d_{LO} / T_s \rfloor$.

Define $u(i) \triangleq E[\Delta[m]\varphi_{LO}[m-i]]$. It can be shown that

$$u(i)=\begin{cases}\dfrac{\sigma_{\theta s}^2}{T}[\min(mT_s,(m-i)T_s+d_{LO})-\max(mT_s-d_{TX},(m-i)T_s)], & 1\le i\le d_2\\ 0, & otherwise\end{cases}$$
$$=\begin{cases}\dfrac{\sigma_{\theta s}^2}{T}[\min(0,d_{LO}-iT)-\max(d_{TX},iT_s)], & 1\le i\le d_2\\ 0, & otherwise\end{cases} \tag{88}$$

Therefore, the third and the fourth terms in (82) becomes:

$$R_1[l]=\sum_{i=1}^{d_2}w[i]u[l+i]=\sum_{i=-\infty}^{\infty}w[i]u[l+i]=\sum_{i=-\infty}^{\infty}w[-i]u[l-i]=w[-l]*u[l] \tag{89}$$

$$R_2[l]=\sum_{i=1}^{d_2}w[i]u[i-l]=R_1[-l]=w[l]*u[-l] \tag{90}$$

Taking the discrete-time Fourier transform of $R_\varphi[l]$ and applying (83)(85)(89)(90) yield the spectrum of the estimation error $\varphi_{TX}[m]$:

$$S_\varphi[f]=S_\Delta[f]+S_{LO}[f]\left|S_w(f)\right|^2-S_u(f)S_w(-f)-S_u(-f)S_w(f) \tag{91}$$

where $S_\Delta[f]$, $S_{LO}[f]$, $S_u(f)$ and $S_w(f)$ are the discrete-time Fourier transform of $R_\Delta[l]$, $R_{LO}[l]$, $u(l)$, and $w[l]$, respectively.

Chapter 8

Conclusion

The focus of this work is to minimize the effects of the phase noise, which is one of the primary factors that limits the performance in many communication systems. The existing work in this area has been carried out separately in the circuit community and the communication and signal processing community. A novel adaptive phase noise compensation scheme, using signal processing techniques together with circuit modifications, is presented for communication transmitters and receivers in this proposal. With the phase noise compensation capabilities provided by the signal processing techniques in the digital backend, the typical high requirement for the oscillator design in the front-end can be relaxed. Satisfactory performance can be achieved by employing a noisier oscillator with the proposed PHN compensation schemes.

For receivers, the proposed phase noise compensation is achieved by using the information provided by an additional signal path that is added to better observe the phase noise. An adaptive decision-directed one-step prediction approach is also introduced. The effectiveness of the proposed scheme is confirmed by analysis and simulation results for a 64-QAM receiver. Lab testing results for a BPSK receiver is

also provided which suggests that the proposed scheme outperforms the conventional schemes.

For communication transmitters, two additional signal paths are added to improve the PHN estimation. The signal from LO Path that has access to the future PHN information is applied as the input of the PHN estimation filter. The TX Path provides the error signal to keep track of the changes in the estimation error. Both paths are downconverted to baseband by self-downconversion, i.e., mixing themselves with the delayed and conjugated replica. The PHN estimation algorithm is derived and adaptive PHN estimation are also devised for transmitter PHN compensation.

Both stationary and Wiener PHN can be compensated effectively by adding the additional paths. The proposed self-down-conversion approach is simple and broadly applicable to various communication systems.

Bibliography

[1] Alexovich, J. R. and Gagliardi, R. M., “The effect of phase noise on noncoherent digital communications”, *IEEE transactions on Communications*, vol. 38, no. 9, pp. 1539-1548, Sept. 1990.

[2] Andreani, P. and Mattisson, S., "On the use of MOS varactors in RF VCOs," *IEEE Journal of Solid-State Circuits*, vol. 35, no. 6, pp. 905-910, June 2000.

[3] Armada, A. G., "Understanding the effects of phase noise in orthogonal frequency division multiplexing (OFDM)," *IEEE Transactions on Broadcasting*, vol. 47, no. 2, pp. 153-159, June 2001.

[4] Ashby, K. B., Koullias, I. A., Finley, W. C., Bastek, J. J., and Moinian, S., “High Q inductors for wireless applications in a complementary silicon bipolar process,” *IEEE Journal of Solid-State Circuits*, vol. 31, no. 1, pp. 4-9, January 1996.

[5] Bahai, A. R. S., Saltzberg, B. R., and Ergen M., *Multi-Carrier Digital Communications Theory and Applications of OFDM (2nd Ed.)*, Springer, 2004.

[6] Bingham, J.A.C., "Multicarrier modulation for data transmission: an idea whose time has come," *IEEE Communications Magazine*, vol. 28, no. 5, pp. 5-14, May 1990.

[7] Castello, R., Erratico, P., Manzini, S., and Sveito, F., "A ±30% tuning range varactor compatible with future scaledtechnologies," *Digest of Technical Papers of the 1998 Symposium on VLSI Circuits*, pp. 34-35, June 1998.

[8] Cimini, L. J., "Analysis and simulation of a digital mobile channel using orthogonal frequency division multiplexing," *IEEE Transactions on Communications*, vol. 33, no.7, pp. 665-675, July 1985

[9] Corvaja, R. and Pupolin, S., “Phase noise effects in QAM sytems,” Proceedings of t*he 8th IEEE International Symposium on Personal, Indoor and Mobile Radio Communications*, vol.2, pp.452-456, Sept 1997.

[10] Cupo, R. L., and Gitlin, R. D., “Adaptive carrier recovery systems for digital data comunications receivers,” *IEEE Journal on Selected Areas in Communications*, vol. 7, no. 9, pp. 1328-1339, Dec. 1989.

[11] Demir, A., “Computing Timing Jitter From Phase Noise Spectra for Oscillators and Phase-Locked Loops With White and 1/f Noise,” *IEEE transactions on Circuits and Systems-I*, vol. 53, no. 9, pp. 1869–1884, Sept. 2006.

[12] Demir, A., Mehrotra, A., and Roychowdhury, J., “Phase noise and timing jitter in oscillators,” *Proceedings of the IEEE Custom Integrated Circuits Conference*, pp. 45-48, May 1998.

[13] Demir, A., Mehrotra, A., and Roychowdhury, J., “Phase noise in oscillators: a unifying theory and numerical methods for characterization,” *IEEE transactions on Circuits and Systems-I*, vol. 47, no. 5, pp. 655–674, May 2000.

[14] Eng, T. and Milstein, L. B., “Partially coherent DS-SS performance in frequency selective multipath fading,” *IEEE transactions on Communications*, vol. 45, no. 1, pp. 110-1118, Jan. 1997.

[15] Fakhfakh, A., Milet-Lewis, N., Deval, Y., and Levi, H., "Study and behavioural simulation of phase noise and jitter in oscillators," *Proceedings of the 2001 IEEE International Symposium on Circuits and Systems (ISCAS '01)*, vol. 5, pp. 323-326, May 2001.

[16] Gitlin, R. D., “Adaptive phase jitter tracker,” U.S. Pat. 4320526, Mar. 16, 1982.

[17] Hajimiri, A., and Lee, T. H., “A general theory of phase noise in electrical oscillators,” *IEEE Journal on Solid-State Circuits*, vol. 33, no. 2, pp. 179-194, Feb. 1998.

[18] Hajimiri, A., and Lee, T. H., “Oscillator phase noise: a tutorial,” *IEEE Journal on Solid-State Circuits*, vol. 35, no. 3, pp. 326-336, March 2000.

[19] Hajimiri, A., and Lee, T., *The Design of Low-Noise Oscillators*, Norwell, MA: Kluwer, 1999.

[20] Haykin, S., *Adaptive Filter Theory*, 3rd Ed., Prentice Hall, 1998

[21] Kailath, T., Sayed, A. H., and Hassibi, B., *Linear Estimation*, Prentice Hall, 2000.

[22] Kim, Y. W., Chae, J. S., and Park, D. C., “Circuit design and performance analysis of carrier recovery loop for digital DBS system in the presence of phase noise,” *IEEE transactions on Broadcasting*, vol. 45, no. 3, pp. 294-302, Sept. 1999.

[23] Lee, T. H., *The Design of CMOS Radio-Frequency Integrated Circuits*, Cambridge University Press; 2nd Ed., 2003

[24] Leeson, D. B., “A simple model of feedback oscillator noise spectrum,” *Proceedings of the IEEE*, vol. 54, no. 2, pp. 329-330, Feb. 1966.

[25] Lindsey, W. C. and Simon, M. K., *Telecommunication Systems Engineering*, Engelwood Cliffs, NJ: Prentice Hall, 1973.

[26] Manton, J. H., "Dissecting OFDM: the independent roles of the cyclic prefix and the IDFT operation," *IEEE Communications Letters*, vol. 5, no. 12, pp. 474-476, Dec. 2001.

[27] Mehrotra, A., "Noise analysis of phase-locked loops," *IEEE transactions on Circuits and Systems-I*, vol. 49, no. 9, pp. 1309-1316, Sept. 2002.

[28] Mendel, J. M., *Lessons in Estimation Theory for Signal Processing*, Communications, and Control (2 edition), Pearson Education POD, March 1995.

[29] Meyr, H., Moeneclaey, M., and Fechtel, S. A., *Digital Communication Receivers*, John Wiley & Sons, 1998.

[30] Nikitopoulos, K., and Polydoros, A., "Compensation schemes for phase noise and residual frequency offset in OFDM systems," *Proceedings of the IEEE Global Telecommunications Conference 2001*, vol. 1, pp. 330-333, 2001.

[31] Oliaei, O., "Extraction of timing jitter from phase noise," *Proceedings of the 2003 International Symposium on Circuits and Systems (ISCAS '03)*, vol. 1, pp. 729-732, May 2003.

[32] Onizawa, T., Mizoguchi, M., Sakata, T., and Morikura, M., "A new simple adaptive phase tracking scheme employing phase noise estimation for OFDM signals," *Proceedings of the IEEE Vehicular Technology Conference VTC Spring 2002*, vol.3, pp. 1252-1256, 2002.

[33] Piazzo, L. and Mandarini, P., "Analysis of phase noise effects in OFDM modems," *IEEE transactions on Communications*, vol. 50, no. 10, pp. 1696-1705, Oct. 2002.

[34] Pollet, T., Van Bladel, M., Moeneclaey, M., "BER sensitivity of OFDM systems to carrier frequency offset and Wiener phase noise," *IEEE Transactions on Communications*, vol. 43, no. 234, pp. 191-193, Feb. 1995.

[35] Poore, R. "Phase noise and Jitter," *Agilent Advanced Design System (ADS) Application Note*, Agilent Technologies, 2001.

[36] Proakis, J. G., *Digital Communications (4th Ed.)*, The McGraw-Hill Companies, 2001.

[37] Proakis, J. G. and Salehi, M., *Communication Systems Engineering*, Prentice Hall, 1994.

[38] Razavi, B., “A study of phase noise in CMOS oscillators,” *IEEE Journal of Solid-State Circuits*, vol. 31, pp. 331–343, Mar. 1996.

[39] Razavi, B., *RF Microelectronics*, Prentice Hall PTR, 1997.

[40] Robertson, P. and Kaiser, S., “Analysis of the effects of the phase noise in OFDM systems,” *Proceedings of the IEEE International Conference. on Communications (ICC95)*, vol. 3, pp. 1652-1657, Jun. 1995.

[41] Rohde, U. L., *Digital PLL frequency Synthesizers: Theory and Design*, Englewood Cliffs, NJ: Prentice-Hall, 1983.

[42] Samori, C., Lacaita, A. L., Zanchi, A., and Pizzolato, F, “Experimental verification of the link between timing jitter and phase noise,” *Electronics Letters*, vol. 34, no. 21, pp. 2024-2025, Oct. 1998.

[43] Simon, V., Senst, A., Speth, M., and Meyr, H., “Phase noise estimation via adapted interpolation,” *Proceedings of the IEEE Global Telecommunications Conference 2001*, vol.6, pp. 3297-3301, 2001.

[44] Slade, G. W., “Effects of local oscillator phase noise on interference rejection capability of CDMA receivers using adaptive antenna arrays,” *IEEE MTT-S International Microwave Symposium Digest*, vol. 2, pp. 1353-1356, June 2002.

[45] Tan, G. L. and Kingsbury, N. G., “Performance degradation of digital modulation schemes caused by random-walk phase noise,” *Proceedings of the IEEE International Conference. on Communications (ICC89)*, vol. 3, pp. 1665-1669, Jun. 1989.

[46] Tomba, L., “On the effect of wiener phase noise in OFDM systems,” *IEEE transactions on Communications*, vol. 46, pp. 580-583, May 1998.

[47] Weinstein, S., and Ebert, P., "Data Transmission by Frequency-Division Multiplexing Using the Discrete Fourier Transform," *IEEE Transactions on Communications*, vol. 19, no.5, pp. 628-634, Oct. 1971.

[48] Yue, C.P. and Wong, S.S., "Design strategy of on-chip inductors for highly integrated RF systems," *Proceedings of the 36th Design Automation Conference*, pp. 982-987, June 1999.

[49] Zhao, L. and Namgoong, W., "A novel adaptive phase noise compensation scheme for communication receivers," *Proceedings of the 2003 IEEE Global Telecommunications Conference (GLOBECOM '03)*, vol. 4, pp. 2274-2279, Dec. 2003.

[50] Zhao, L. and Namgoong, W., "Performance of a novel phase noise compensation scheme for communication receivers in the presence of Wiener phase noise," *Proceedings of the 2004 IEEE International Conference on Acoustics, Speech, and Signal Processing (ICASSP '04)*, vol. 4, pp. 1025-1028, May 2004.

[51] Zhao, L. and Namgoong, W., "Communication transmitter phase noise compensation based on the self-downconversion architecture," *Proceedings of the 2005 IEEE International Conference on Communications (ICC 2005)*, vol. 3, pp. 2075-2079, May 2005.

[52] Zhao, L. and Namgoong, W., "A novel phase-noise compensation scheme for communication receivers," *IEEE Transactions on Communications*, vol. 54, no. 3, pp. 532-542, March 2006.

Appendix A

The (i,j)th element of $\mathbf{R}_1$ for $i, j \in [1, N_1]$ in (23) is

$$\begin{aligned}\mathbf{R}_1(i,j) &= E\left[(\hat{\theta}_{k-i|k-i} - \theta_o)(\hat{\theta}_{k-j|k-j} - \theta_o)\right] \\ &= E\left[\left(\phi[k-i] + \mathrm{Im}[\xi_{k-i}](1-\mathrm{Re}[\xi_{k-i}]\right)\left(\phi[k-j] + \mathrm{Im}[\xi_{k-j}](1-\mathrm{Re}[\xi_{k-j}]\right)\right]. \quad (92) \\ &= R_\phi((i-j)T) + \delta(i-j)(\frac{1}{2}\sigma_{w1}^2 E[\frac{1}{|a_n|^2}] + \frac{1}{4}\sigma_{w1}^4 E[\frac{1}{|a_n|^4}])\end{aligned}$$

where $R_\phi(\tau)$ is the correlation for stationary PHN $\phi(t)$. The last term in (92) comes from the variance of the noise term $\mathrm{Im}[\xi_n](1-\mathrm{Re}[\xi_n])$ in (19):

$$\begin{aligned}E\left[\left(\mathrm{Im}[\xi_{k-i}](1-\mathrm{Re}[\xi_{k-i}])\right)^2\right] &= E\left[E\left[\left(\mathrm{Im}[\xi_{k-i}]\right)^2 + \left(\mathrm{Im}[\xi_{k-i}]\right)^2\left(\mathrm{Re}[\xi_{k-i}]\right)^2\right.\right. \\ &\qquad \left.\left. -2\left(\mathrm{Im}[\xi_{k-i}]\right)^2 \mathrm{Re}[\xi_{k-i}] \mid a,\ \theta[k-i]\right]\right] \quad . \quad (93) \\ &= \frac{1}{2}\sigma_{w1}^2 E[\frac{1}{|a_n|^2}] + \frac{1}{4}\sigma_{w1}^4 E[\frac{1}{|a_n|^4}]\end{aligned}$$

The ith element in $\mathbf{p}_1$ for $i \in [1, N_1]$ is

$$\begin{aligned}\mathbf{p}_1(i) &= E[(\hat{\theta}_{k-i|k-i} - \theta_o)(\theta[k] - \theta_o)] \\ &= E\left[\left(\phi(m_0T_s + (k-i)T - t_1) + \mathrm{Im}[\xi_{k-i}](1-\mathrm{Re}[\xi_{k-i}])\right)\cdot\left(\phi(m_0T_s + kT - t_1)\right)\right]. \quad (94) \\ &= E[\phi(m_0T_s + (k-i)T - t_1)\phi(m_0T_s + kT - t_1)] = R_\phi(iT)\end{aligned}$$

Noticing that the additive noise in Path I and Path II are independent, and that the PHN is independent to the additive noise, the (i,j)th element of $\mathbf{R}_{12}$ for $i \in [1, N_1]$ and $j \in [1, N_2 + D + 1]$ is

$$
\begin{aligned}
\mathbf{R}_{12}(i,j) &= E[\theta[k-i]\varphi[k+D+1-j]] \\
&= E[\big(\theta_o + \phi(m_0T_s + (k-i)T - t_1)\big)\cdot \\
&\quad \big(\gamma + \theta((k+D+1-j)T) - \theta((k+D+1-j)T - t_2)\big)] \\
&= \theta_o\gamma + R_\phi((D+1+i-j)T) - R_\phi((D+1+i-j)T + t_1 - t_2)
\end{aligned} \quad . \tag{95}
$$

The (i,j)th element of $\mathbf{R}_2$ for $i, j \in [1, N_2 + N_3 + 1]$ is given by

$$
\begin{aligned}
\mathbf{R}_2(i,j) &= E[\varphi[k+D+1-i]\varphi[k+D+1-j]] \\
&= \gamma^2 + 2R_\phi((i-j)T) - R_\phi((i-j)T - t_2) \\
&\quad -R_\phi((i-j)T + t_2) + \delta(i-j)\left(\frac{1}{2}\sigma_{w2}^2 + \frac{1}{4}\sigma_{w2}^4\right)
\end{aligned} \quad , \tag{96}
$$

where the last term is the variance of the noise present in Path II similar to (27).

The ith element in $\mathbf{p}_2$ for $i \in [1, N_2 + D + 1]$ is

$$
\begin{aligned}
\mathbf{p}_2(i) &= E[\varphi[k+D+1-i]\theta[k]] \\
&= E\Big[\big(\theta_o + \phi(m_0T_s + (k-i)T - t_1) + \mathrm{Im}[\varsigma_{k-i}](1 - \mathrm{Re}[\varsigma_{k-i}])\big) \\
&\quad \big(\theta_o + \phi(m_0T_s + kT - t_1)\big)\Big] \\
&= \theta_o\gamma + R_\phi((D+1-i)T) - R_\phi((D+1-i)T - t_2)
\end{aligned} \quad . \tag{97}
$$

Appendix B

The PHN component in the (i,j)th element of $\mathbf{R}_1$ for $i, j \in [1, N_1]$ in (43) is

$$\begin{aligned}
\mathbf{R}_1(i,j) &= E\left[\left(\phi[k-i]-\frac{1}{N}\sum_{l=1}^{N}\phi[k-l]\right)\left(\phi[k-j]-\frac{1}{N}\sum_{l=1}^{N}\phi[k-l]\right)\right] \\
&= \sigma_\theta^2\left[\min(M-i,M-j)-\frac{1}{N}\sum_{l=1}^{N}\min(M-i,M-l)\right. \\
&\quad \left.-\frac{1}{N}\sum_{l=1}^{N}\min(M-j,M-l)+\sum_{l=1}^{N}\sum_{m=1}^{N}\min(M-l,M-m)\right] \\
&= \sigma_\theta^2\left[\frac{1}{N}\sum_{l=1}^{N}\max(i,l)+\frac{1}{N}\sum_{l=1}^{N}\min(j,l)-\max(i,j)-\sum_{l=1}^{N}\sum_{m=1}^{N}\max(l,m)\right] \\
&= \sigma_\theta^2[(N+1)(2N+1)/(6N)+(i^2+i+j^2+j)/(2N)-\max(i,j)]
\end{aligned} \tag{98}$$

Accounting for the noise term $arctg(\mathrm{Im}[\xi_n](1-\mathrm{Re}[\xi_n]))$ in $\hat{\theta}_{n|n}$, (98) becomes (43).

The ith element in $\mathbf{p}_1$ for $i \in [1, N_1]$ is

$$\begin{aligned}
\mathbf{p}_1(i) &= E\left[\left(\theta[k-i]-\frac{1}{N}\sum_{l=1}^{N}\theta[k-l]\right)\left(\theta[k]-\frac{1}{N}\sum_{l=1}^{N}\theta[k-l]\right)\right] \\
&= \mathbf{R}_1(i,0) = \sigma_\theta^2[(N+1)(2N+1)/(6N)+(i^2-i)/(2N)-i]
\end{aligned} \tag{99}$$

Similar to (36), $\mathbf{R}$ can be divided into blocks, where $\mathbf{R}_1$ has been calculated in (98).

The (i,j)th element of $\mathbf{R}_{12}$, $i \in [1, N_1]$ and $j \in [1, N_2 + D + 1]$, is

$$
\begin{aligned}
\mathbf{R}_{12}(i,j) &= E\left[\left(\theta[k-i]-\frac{1}{N}\sum_{l=1}^{N}\theta[k-l]\right)\varphi(k+D+1-j)\right] \\
&= E\left[\left(\phi[k-i]-\frac{1}{N}\sum_{l=1}^{N}\phi[k-l]\right)\right. \\
&\quad \left.\left(\phi\left(m_sT_s+(k+D+1-j)T\right)-\phi\left(m_sT_s+(k+D+1-j)T-t_2\right)\right)\right] \\
&= \sigma_\theta^2\left[\max(i,j-D-1+\frac{t_1-t_2}{T})+\frac{1}{N}\sum_{l=1}^{N}\max(l,j-D-1-\frac{t_1}{T})\right. \\
&\quad \left.-\max(i,j-D-1-\frac{t_1}{T})-\frac{1}{N}\sum_{l=1}^{N}\max(l,j-D-1+\frac{t_1-t_2}{T})\right]
\end{aligned}
\tag{100}
$$

The PHN component in (i,j)th element of $\mathbf{R}_2$, $i\in[1,N_2+D+1]$ and $j\in[1,N_2+D+1]$, is:

$$
\begin{aligned}
\mathbf{R}_2(i,j) &= E\left[\left(\phi\left(m_sT_s+(k+D+1-i)T\right)-\phi\left(m_sT_s+(k+D+1-i)T-t_2\right)\right)\right. \\
&\quad \left.\left(\phi\left(m_sT_s+(k+D+1-j)T\right)-\phi\left(m_sT_s+(k+D+1-j)T-t_2\right)\right)\right] \\
&= \sigma_\theta^2\left[\min(M+D+1-i+\frac{t_1}{T},M+D+1-j+\frac{t_1}{T})\right. \\
&\quad -\min(M+D+1-i+\frac{t_1}{T},M+D+1-j+\frac{t_1-t_2}{T}) \\
&\quad -\min(M+D+1-i+\frac{t_1-t_2}{T},M+D+1-j+\frac{t_1}{T}) \\
&\quad \left.+\min(M+D+1-i+\frac{t_1-t_2}{T},M+D+1-j+\frac{t_1-t_2}{T})\right] \\
&= \sigma_\theta^2\left[\max(i,j+\frac{t_2}{T})+\max(i+\frac{t_2}{T},j)-2\max(i,j)-\frac{t_2}{T}\right]
\end{aligned}
\tag{101}
$$

Accounting for the noise term $arctg(\mathrm{Im}[\xi_n](1-\mathrm{Re}[\xi_n]))$, (101) becomes

$$
\begin{aligned}
\mathbf{R}_2(i,j) &= \sigma_\theta^2\left[\max(i,j+\frac{t_2}{T})+\max(i+\frac{t_2}{T},j)-2\max(i,j)-\frac{t_2}{T}\right] \\
&\quad +\delta(i-j)\left(\frac{1}{2}\sigma_{w2}^2+\frac{1}{4}\sigma_{w2}^4\right)
\end{aligned}
\tag{102}
$$

$\mathbf{p}$ is also expressed in blocks as in (37), where $\mathbf{p}_1$ has been calculated in (99). Noticing the independence between the noise terms in Path I and Path II, $\mathbf{p}_2$ can be obtained by

$$
\begin{aligned}
\mathbf{p}_2(i) &= E\left[\varphi(k+D+1-j)\left(\theta[k]-\frac{1}{N}\sum_{l=1}^{N}\theta[k-l]\right)\right] \\
&= E\Big[\Big(\phi\big(m_oT_s+(k+D+1-i)T\big)-\phi\big(m_oT_s+(k+D+1-i)T-t_2\big)\Big) \\
&\quad \left(\phi\big(m_oT_s+kT-t_1\big)-\frac{1}{N}\sum_{l=1}^{N}\phi\big(m_oT_s+(k-l)T-t_1\big)\right)\Big] \\
&= \sigma_\theta^2\Bigg[\min(M+D+1-i+\frac{t_1}{T},M) \\
&\quad -\min(M+D+1-i+\frac{t_1-t_2}{T},M) \\
&\quad -\frac{1}{N}\sum_{l=1}^{N}\min(M+D+1-i+\frac{t_1}{T},M-l) \\
&\quad +\frac{1}{N}\sum_{l=1}^{N}\min(M+D+1-i+\frac{t_1-t_2}{T},M-l)\Bigg] \\
&= \sigma_\theta^2\Bigg[\max(i-D-1+\frac{t_1-t_2}{T},0)+\frac{1}{N}\sum_{l=1}^{N}\max(l,i-D-1-\frac{t_1}{T}) \\
&\quad -\max(i-D-1-\frac{t_1}{T},0)-\frac{1}{N}\sum_{l=1}^{N}\max(i-D-1+\frac{t_1-t_2}{T},l)\Bigg]
\end{aligned}
\tag{103}
$$

For $\mathbf{R}_{12}$ and $\mathbf{p}_2$, the values of the summation depend on the relation between t_1 and t_2. Although close form expression can be obtained, it is too complex and not worth pursuing, since it can be computed numerically easily.